

SCIENCE
APPLICATIONS
INCORPORATED

JAR FILE # 490

POST-TEST EVALUATION OF
NTS MULTIPLE FRACTURE/MINEBACK EXPERIMENTS

UGR FILE # 490

Sub-Task Technical Report
EGSP Support Contract Task 21
Contract No. DE-AT21-78MC08216

Prepared by

Timothy G. Barbour

Science Applications, Incorporated
1726 Cole Blvd., Suite 350
Golden, Colorado 80401

December 1980

Prepared for

Eastern Gas Shales Project
Morgantown Energy Technology Center
Collins Ferry Road
Morgantown, West Virginia 26505

EXECUTIVE SUMMARY

As a part of Science Applications' support of the Eastern Gas Shales Project, a research program is being conducted to evaluate unconventional **wellbore** stimulation technologies. Included in this effort is the development of numerical models to describe and predict laboratory experiment and field demonstration results. The numerical model development is also being used in parameter sensitivity analyses to determine the importance of various aspects of the dynamic **wellbore** loading phenomenology.

This report presents the results of a computational investigation of three NTS Multi-Frac Test Series experiments. The evaluation was performed to compare the results as computed by the **STEALTH/CAVS** codes against the field results as observed by mineback. Field record data of the **borehole** cavity pressure history were approximated and applied as **wellbore** boundary pressure-time histories in the one-dimensional cylindrical geometry calculations. Stresses and material property data for the stimulated ash-fall tuff were modeled to replicate *in situ* conditions. The three field experiments that were modeled are:

- Unaugmented Dynafrac; a small-diameter explosive decoupled with a water pad,
- Single-shot Kinefrac; a small-diameter propellant charge with a pressurized water pad, and
- Gas-Frac; a full-diameter charge of progressively burning propellant.

Models of compaction and yielding were included in the tuff constitutive description. Tensile fracture of the tuff, as described by the CAVS model was described, including the influence of gas or water penetration and pressurization of the induced cracks.

Results of the computational evaluation of the three treatments addressed are as follows:

- 1) In all calculations, the computed radial acceleration, radial stress and tangential stress histories at the instrumentation locations were about an order-of-magnitude larger than the field records. The discrepancy is predominantly attributable to the fact that the calculations were one-dimensional descriptions of a three-dimensional event. Also, the material descriptions used to model the water saturated tuff were probably not completely adequate. The material properties were obtained from quasi-static laboratory experiments where drainage of the pore fluid was allowed, in contrast to the dynamic probably undrained conditions of the field tests.
- 2) The Gas-Frac shot produced peak borehole pressures of several hundred mega-pascals (an order-of-magnitude larger than the Kinefrac shot and about three times that of the Dynafrac shot). The high peak cavity pressures induced considerable compaction of the tuff near the wellbore, as computed in the numerical simulation. This compaction was not observed in the field and suggests inappropriate compaction and/or yield models for the tuff, at least at these high stresses. The computed radial fracture development (using the CAVS model of tensile failure) was, in an absolute sense, somewhat less than the field results, although in a relative sense (when compared to the Kinefrac and Dynafrac simulations) is moderately good. The maximum computed radial crack length was about 1.5 meters. Observed field results indicated concentrated cracks (radial and circumferential) to about 0.5 meter; a few radial radials to about 1.5 meters; and a major crack to about 6 meters.
- 3) The Kinefrac shot produced peak borehole pressures of several tens of mega-pascals. Only minimal permanent wellbore expansion was observed upon mineback. Compute results compare quite favorably. The single Kinefrac test produced radial cracks extending to a maximum distance of about 1 meter. All cracks were tight. The compute crack void strain (a measure of the crack width) is minimal and in agreement with observed results. The distribution of radial cracks, as computed, is also in good agreement with observed results. The maximum length of computed radial cracks is about 0.3 meter.
- 4) The unaugmented Dynafrac shot did not produce any significant crack development. The wellbore was enlarged by 15 - 35 percent due to yielding of the tuff. The computed wellbore expansion was about an order-of-magnitude less than the observed results. The computed maximum radial fracture extends to about 6 inches with very minimal crack void development or fluid penetration into the cracks. This compares quite well with the observed results.

PREFACE

The Eastern Gas Shales Project (EGSP) of the Department of Energy (DOE) has the goal of examining marginal gas resources and to determine what methods would be required to extract vast amounts of natural gas trapped in eastern Devonian shales. As part of this project the Morgantown Energy Technology Center (METC) is conducting a research program to evaluate stimulation technologies in these relatively impermeable gas shales. One aspect of the program is concerned with numerical model development which would be used in assessing the suitability of various stimulation treatments. Part of this study is being conducted by Science Applications, Incorporated (SAI) under contract to METC. This report presents the results of a comparative evaluation between observed borehole expansion and fracture development in the Nevada Test Site (NTS) Multi-Frac Test Series and the results of SAI's STEALTH/CAVS computational model to simulate these experiments.

CONTENTS

| | <u>Page</u> |
|---|-------------|
| SECTION 1 | |
| INTRODUCTION | 1 |
| 1.1 NTS Multi-Frac Test Series | 1 |
| 1.2 Post-Test Evaluation | 2 |
| SECTION 2 | |
| COMPUTATIONAL EVALUATION OF NTS EXPERIMENTS | 3 |
| 2.1 Ash-Fall Tuff Material Properties | 4 |
| 2.2 Gas-Frac Experiment | 6 |
| 2.3 Kinefrac (Single Shot) Experiment | 9 |
| 2.4 Dynafrac (Unaugmented) Experiment | 10 |
| SECTION 3 | |
| SUMMARY AND CONCLUSIONS | 12 |
| REFERENCES | 15 |
| TABLES | 17 |
| FIGURES | 20 |

LIST OF TABLES

| <u>Table</u> | | <u>Page</u> |
|--------------|---|-------------|
| 1 | NTS G-Tunnel Ash-Fall Tuff Material Properties..... | 17 |

LIST OF FIGURES

| <u>Figure</u> | <u>Page</u> |
|---------------|---|
| 1 | NTS G-Tunnel Ash-Fall Tuff Compaction.....20 |
| 2 | NTS G-Tunnel Ash-Fall Tuff Yield Envelope..... 21 |
| 3 | One-dimensional Calculational Model (Geometry and Initial Conditions) for NTS Multi-Frac Experiments..... 22 |
| 4 | Gas-Frac (GF-4) Cavity Pressure Record and Simulated Pressure Pulse..... 23 |
| 5 | Kinefrac (GF-5) Cavity Pressure Record and Simulated Pressure Pulse..... 24 |
| 6 | Dynafrac (GF-7) Cavity Pressure Record and Simulated Pressure Pulse..... 25 |
| 7 | Gas-Frac - Radial Acceleration, Radial Stress and Tangential Stress at Wellbore Wall (<u>with</u> tuff compaction and yielding)a 26 |
| 8 | Gas-Frac - Radial Acceleration, Radial Stress and Tangential Stress at Approximately 1.5 Feet from Wellbore Center (<u>with</u> tuff compaction and yielding)..... 27 |
| 9 | Gas-Frac - Radial Acceleration, Radial Stress and Tangential Stress at Approximately 3.0 Feet from Wellbore Center (<u>with</u> tuff compaction and yielding)..... 28 |
| 10 | Gas-Frac - Radial Acceleration, Radial Stress and Tangential Stress at Approximately 6.0 Feet from Wellbore Center (<u>with</u> tuff compaction and yielding)..... 29 |
| 11 | Gas-Frac - Wellbore Expansion (<u>with</u> tuff compaction and yielding) 30 |
| 12 | Gas-Frac - Crack Void Strain Distribution at 2.5 and 10 Milliseconds (<u>with</u> tuff compaction and yielding)..... 31 |
| 13 | Gas-Frac - CAVS Fracture Plot at 3 and 5 Milliseconds (<u>with</u> tuff compaction and yielding)..... 32 |
| 14 | Gas-Frac - Radial Acceleration, Radial Stress and Tangential Stress at Wellbore Wall (<u>without</u> tuff compaction or yielding) 33 |

LIST OF FIGURES
(Continued)

| <u>Figure</u> | | <u>Page</u> |
|---------------|---|-------------|
| 15 | Gas-Frac - Radial Acceleration, Radial Stress and Tangential Stress at Approximately 1.5 Feet from Wellbore Center (<u>without</u> tuff compaction or yielding) | 34 |
| 16 | Gas-Frac - Radial Acceleration, Radial Stress and Tangential Stress at Approximately 3.0 Feet from Wellbore Center (<u>without</u> tuff compaction or yielding) | 35 |
| 17 | Gas-Frac - Radial Acceleration, Radial Stress and Tangential Stress at Approximately 6.0 Feet from Wellbore Center (<u>without</u> tuff compaction or yielding) | 36 |
| 18 | Gas-Frac - Wellbore Expansion (<u>without</u> tuff compaction or yielding) | 37 |
| 19 | Gas-Frac - Crack Void Strain Distribution and Crack Internal Pressure Profile at 10 Milliseconds (<u>without</u> tuff compaction or yielding) | 38 |
| 20 | Gas-Frac - CAVS Fracture Plot at 1 and 2 Milliseconds (<u>without</u> tuff compaction or yielding)..... | 39 |
| 21 | Gas-Frac - CAVS Fracture Plot at 3 and 5 Milliseconds (<u>without</u> tuff compaction or yielding)..... | 40 |
| 22 | Kinefrac - Radial Acceleration, Radial Stress and Tangential Stress at Wellbore Wall | 41 |
| 23 | Kinefrac - Radial Acceleration, Radial Stress and Tangential Stress at Approximately 1.5 Feet from Wellbore Center | 42 |
| 24 | Kinefrac - Radial Acceleration, Radial Stress and Tangential Stress at Approximately 3.0 Feet from Wellbore Center | 43 |
| 25 | Kinefrac - Radial Acceleration, Radial Stress and Tangential Stress at Approximately 6.0 Feet from Wellbore Center | 44 |

LIST OF FIGURES
(Continued)

| <u>Figure</u> | <u>Page</u> |
|---------------|--|
| 26 | Kinefrac - Wellbore Expansion.....45 |
| 27 | Kinefrac - Crack Void Strain Distribution and Crack Internal Pressure Profile at 16 Milliseconds.....46 |
| 28 | Kinefrac - CAVS Fracture Plot at 3 and 5 Milliseconds..... 47 |
| 29 | Kinefrac - CAVS Fracture Plot at 10 and 16 Milliseconds..... 48 |
| 30 | Dynafrac - Radial Acceleration, Radial Stress and Tangential Stress at Wellbore Wall..... 49 |
| 31 | Dynafrac - Radial Acceleration, Radial Stress and Tangential Stress at Approximately 1.5 Feet from Wellbore Center..... 50 |
| 32 | Dynafrac - Radial Acceleration, Radial Stress and Tangential Stress at Approximately 3.0 Feet from Wellbore Center..... 51 |
| 33 | Dynafrac - Radial Acceleration, Radial Stress and Tangential Stress at Approximately 6.0 Feet from Wellbore Center..... 52 |
| 34 | Dynafrac - Well Expansion..... 53 |
| 35 | Dynafrac - Crack Void Strain Distribution and Crack Internal Pressure Profile at 0.25 Milliseconds.....54 |
| 36 | Dynafrac - Crack Void Strain Distribution and Crack Internal Pressure Profile at 2.0 Milliseconds.....55 |
| 37 | Dynafrac - CAVS Fracture Plot at and 2.0 Milliseconds..... 56 |

1. INTRODUCTION

1.1 NTS Multi-Frac Test Series

The Multi-Frac Test Series, recently completed at the Nevada Test Site (NTS) had two purposes: (1) evaluate and compare five tailored-pulse-loading stimulation treatments under *in situ* conditions to determine the ability of each to produce multiple fractures and to enhance formation permeability and (2) provide data for testing and verification of various numerical modeling schemes presently being developed to describe the complex behavior of dynamic **wellbore** stimulation in a deep wellbore.

Five full-scale shots were performed in a thick ash-fall tuff formation. Conducted in horizontal boreholes drilled from a tunnel under 430 meters of overburden, the test site provided both realistic *in situ* conditions and access to the test zone by **mineback** permitting direct observation of the test results. Data for model verification were collected during each test using stress gages and accelerometers embedded in instrumentation holes in the surrounding rock. Each test monitored the cavity pressure using transducers in each borehole. Pre-test and post-test evaluation included TV and caliper logs and permeability measurements. Laboratory experiments were performed on the core obtained from the boreholes to determine the static and dynamic material properties. The combination of the site specific material data, actual cavity pressure, rock stress and acceleration data and direct observation of the induced fractures provided the necessary information required to numerically model each test. The five tailored-pulse-loading concepts tested involved:

- a) a small-diameter explosive decoupled with a water pad,
- b) a small-diameter decoupled explosive with water pad and an added propellant booster,
- c) a small-diameter propellant charge with a pressurized water pad,
- d) three successive shots of case c, and
- e) a full-diameter charge of progressively burning propellant.

A thorough discussion of the specific test configurations and an evaluation of the test results are presented by Schmidt (12, 13, 14). Post-test evaluation of the numerical models that are currently being used to describe the effects of dynamic **wellbore** stimulation is currently in progress. This report presents an evaluation of three of the Multi-Frac experiments: a) the unaugmented Dynafrac (11) experiment (test a above), b) the single shot Kinefrac (8) experiment (test c above), and c) the Gas-Frac (15) experiment (test e above).

1.2 Post-Test Evaluation

A computational evaluation of three Multi-Frac experiments has been performed to compare the observed field results against the computed results by the **STEALTH/CAVS** numerical code and fracture description. Two of the experiments were not considered in the evaluation; the augmented Dynafrac experiment (test b above) because of its unsuccessful completion, and the multiple Kinefrac experiment (test d above) because it represents a **duplication** of the single Kinefrac shot. The **STEALTH*** (9) finite-difference codes **were** used to replicate the rock motion as a result of the energy release and reaction product expansion of the unaugmented Dynafrac, Gas-Frac, and single Kinefrac stimulation treatments. Constitutive descriptions of the rock's response included yielding, compaction, and tensile failure. Tensile failure was described using the **CAVS (5,10)** cracking and void strain model. Field records of the **borehole** cavity pressure histories were approximated and applied as boundary histories to the computational models to simulate the induced stress waves. Fluid flow from the **wellbore** into the induced fractures is modeled within the context of **CAVS**.

* **STEALTH** (**S**olids and **T**hermal **H**ydraulic code for **E**PRI adapted from Lagrange **T**OOBY and **H**EMP) developed under EPRI contract RP-307.

2. COMPUTATIONAL EVALUATION OF NTS MULTI-FRAC EXPERIMENTS

A method which is becoming increasingly useful in the analysis of dynamic rock fracture and fragmentation utilizes stress wave propagation codes. These codes solve by finite-difference techniques the equations of continuum mechanics and, with appropriately defined constitutive equations describing the rock's response to the applied load, serve as a unique means of analyzing non-linear, inelastic, dynamic events.

An instance where these codes have proven particularly useful is in the study of the rock's response to the dynamic loading imparted in a **wellbore** by an explosive stimulation treatment. With explicit finite-difference codes such as STEALTH, the physical phenomena controlling the dynamic events that occur during explosive **wellbore** loading can be better understood with appropriately designed parameter sensitivity analyses. Sensitivity calculations used to establish the relative importance on fracture development of parameters, such as the loading and decay rates of applied **wellbore** pulses, the rock's deformational and failure description, and in situ stress and geometry conditions, have been addressed in previous reports of SAI's current evaluation of unconventional **wellbore** stimulation (2, 3, 4).

In addition to sensitivity analyses, it is possible to perform comparative evaluations of field demonstrations of unconventional **wellbore** stimulation treatments. The recently completed NTS Multi-Frac Test Series is a part of METC's current EGSP program and provides an ideal case for comparative analysis between the observed field results and the results computed by present computational models. In addition to direct **mineback** observations, the NTS experiments have provided stress and acceleration measurements in the rock adjacent to each **wellbore** and pressure histories in the **wellbore** cavities. These **measurements** provide a record of the loading conditions which produced the observed results.

Material properties of the NTS G-Tunnel ash-fall tuff are summarized first. The computational model used in the calculations and the applied **wellbore** pressure histories, which approximate the field records, are then presented followed by calculated fracture and **wellbore** yielding results.

2.1 Ash-Fall Tuff Material Properties

The proper execution of the calculations described herein required suitable material properties of the NTS tuff. As the existing data on the mechanical properties of the G-Tunnel tuff is quite limited, it has been necessary to carefully review existing data on the tuff and to generate additional data as required. The review, experiments and evaluation have been conducted by SAI and summarized in a recent report by Blanton, et al. (6). Principal conclusions of this effort **are** as follows:

- The yield surface defined by triaxial experiments for the G-Tunnel tuff is significantly lower from that defined for other tuff beds at the NTS.
- Direct-pull tensile strength data obtained within the SAI testing program compares favorably with that obtained by Sandia on the same tuff bed.
- The tensile strength of this rock, although quite variable, is moderately low with values on the order of 1.6 MPa being typical.
- Fracture **energy values** measured for the G-Tunnel tuff, averaging $\sim 9 \text{ J/m}^2$, are quite low as compared to most other rock types, and are a measure of the very fragile nature of the rock.
- Dynamic experiments employing modified Split-Hopkinson-Bar techniques, indicate that the dynamic strength of this rock is only slightly higher than the static strength.
- The dynamic yield data suggests that quasi-statically determined yield surfaces would be suitable for inclusion in calculations to evaluate various dynamic stimulation **creations** in the NTS tuff.
- The dynamic data reveal that the sample deformation is characterized by an initial compaction followed by sample bulking (dilatancy) associated with failure.
- As the relationships between compaction, yielding and failure mode will depend strongly upon pore-pressure effects, as controlled by the degree of sample saturation, additional experimental data will be required to completely describe the importance of saturation.

Table 1 is a summary of the tuff material properties used in the calculations of this report and was compiled from Reference . The in situ density is only 1800 kg/m^3 because a significant portion of the bulk material is water. The tuff has a porosity of about 40% and it is water-saturated. The pores are not well connected, however, with permeabilities ranging from 0.01 to 0.80 md. The water that saturates the pores will have a significant influence on the experimentally determined compressibility and yield surface depending on whether or not the sample is allowed to drain during loading. Under dynamic loading conditions, the low permeability also could cause pore pressures to build up thus reducing the effective stresses. These conditions must be kept in mind in analyzing the mechanical data and interpreting the computed compaction and yielding that occurs during the numerical simulations.

The constitutive behavior typical of the tuff's compressibility is shown in Figure 1. The dashed line on the figure defines the model used in the calculations and represents an approximation of the typical compaction behavior obtained from hydrostatic compression tests. The relatively low slope for volumetric strains less than 1% is due to closing of microflaws and is typical behavior for most rocks at low stresses. Between 3 and 30 MPa the curves steepen and become linear. During this range the rock behaves elastically and slope of the curve is the bulk modulus. An average bulk modulus for 14 determinations is approximately 2.1 GPa. Between 30 and 50 MPa of hydrostatic stress the slope begins to decrease probably representing the onset of pore collapse. When the pressure is compressive, unloading and reloading as defined by the computational model (dashed line of Figure 1) allows for irretrievable compaction by unloading and reloading along a linear path defined by the bulk modulus. When the pressure is tensile, unloading and reloading occurs along a linear path defined by the initial slope of the compressibility curve when the pressure and volumetric strain are zero. Tensile pressures in the computational model will not be of significant magnitude or maintained for very long because of the tensile stress relaxation that is modeling within the CAVS tensile failure model.

The two test results, as shown in Figure 1 and as mentioned above, are typical results. The results, however, are for tests in which the pore water of the specimen was allowed to drain during the quasi-static compression. If

drainage was prohibited a stiffer response would be expected. The rapidness of the dynamic compression expected near the wellbore, during the explosive stimulation treatments considered in this report, would probably not allow sufficient time for pore fluid drainage. The computational model of compressibility, therefore, might be better described with a stiffer modulus than that shown in Figure 1.

The results of fifteen quasi-static differential compression tests performed by Atkinson-Nolan (A-N) and Associates (1) for SAI were used to generate a yield envelope for the G-Tunnel tuff. The results of these tests are shown in Figure 2. A yield envelope for another tuff at the NTS, as defined by Terra Tek (7) is shown in Figure 2 and is designated TT. Both pressure dependent yield surfaces are shown to indicate site-to-site variability of the NTS tuff. The results of the tests by Atkinson and Nolan are for tests in which the pore water of the specimen was allowed to drain during the quasi-static loading. For the same reasons given above prohibiting drainage of the specimen pore fluids, which is likely during dynamic compression, will increase the yield strength. For these calculations, the yield envelope defined by Terra Tek and shown in Figure 2 is used as the computational model. Comparison calculations were performed for the Gas-Frac experiment using the yield envelope descriptions of Atkinson-Nolan, Terra Tek and a constant, very high yield strength to determine the influence on plastic flow near the **wellbore** and on tensile fracture development.

2.2 Gas-Frac Experiment

The Gas-Frac **wellbore** stimulation treatment developed by Sandia Laboratories (15) consists of a gas-producing, progressively-burning propellant with a rise time suitable for the initiation and propagation of multiple fractures while avoiding the near-wellbore damage. The concept provides for 1) a **full-diameter** charge, 2) lightweight gas products from the propellant itself, rather than water, are pushed into the created fractures, and 3) a progress burning propellant in which the burning rate increases as the material is consumed. Specific NTS field test set-up and data records are presented in References 12, 13 and 14.

Figure 3 is a schematic of the one-dimensional cylindrical geometry calculational model used in simulating the Gas-Frac experiment (and the other NTS experiments considered in this report). Initial conditions of stress were defined, as shown in Figure 3, to replicate the measured in situ stresses for the G-Tunnel area in Rainier Mesa at the NTS. The stimulation treatments were run in horizontal, 15 cm holes drilled 12.2 m deep from the tunnel. The overburden stress in the vicinity of the tunnel is 8.6 MPa. The minimum horizontal principal stress is 5.4 MPa and is oriented at 15° to the drilled holes. The maximum horizontal principal stress is 10.3 MPa. One-dimensional analysis does not allow distinction of radial stress anisotropy, thus an average of 8.6 and 10.3 MPa (9.45 MPa) was used to represent to initial radial plane stress. A constant boundary pressure-history is applied at the outer boundary of the model which is at 30 meters. Field record pulses are approximated and applied as boundary pressure-time histories at the **wellbore** wall. The actual field record of the Gas-Frac cavity pressure (12) and the approximated pulse (heavy dashed line) used in the simulation are shown in Figure 4. Equivalent pulses for the Kinefrac and Dynafrac shots are shown in Figures 5 and 6, respectively.

The material properties of the tuff defined in the model, as mentioned above, are summarized in Table 1. The compaction model is shown in Figure 1 and the yield model (designated TT) is shown in Figure 2. Because of the high peak cavity pressures (several hundred MPa) experienced in the Gas-Frac experiment considerable compaction/yielding was computed. The yielding was not observed in the field test and suggests that the material models representing the Figure 1 and 2 behavior are inappropriate in this range of induced stresses. As mentioned in the discussion on the ash-fall tuff material properties (Section 2.1) the dynamic field response and the laboratory measured quasi-static response are based on different conditions of water drainage of the saturated tuff (40% porous). The compaction and yield models probably represent a less stiff and weaker response than the in situ behavior, **partially** explaining the discrepancy between the **computed** and observed results. As a comparison, two calculations were performed for the Gas-Frac evaluation; one with yielding plus compaction and one which simulated a totally elastic response. The results of these two computations are summarized below.

Figures 7 through 13 are results from the Gas-Frac simulation which allowed compaction and yielding of the tuff. Figures 14 through 21 are equivalent plots for the simulation that was elastic. Figures 7 and 14 are time histories of radial acceleration, radial stress and tangential stress at the **wellbore** wall for the two calculations. Figures 8 and 15 are equivalent history plots at 1.5 feet from the **wellbore** center. Figures 9 and 16 are plots at 3.0 feet and Figures 10 and 17 are at 6.0 feet from the **wellbore** center. In comparing the computed results against the field records of acceleration and stress at the above mentioned radial distances, the computed results in these two calculations and the others of this evaluation are an order-of-magnitude larger. Results of the Gas-Frac stressmeter and accelerometer data indicate that the stresses are more than an order-of-magnitude larger than calculated from assumptions of a static **borehole** pressure. The discrepancy may be explained by substantial gas penetration into induced fractures which resulted from this treatment.

An indication of the yielding of the near **wellbore** tuff is shown in the **wellbore** expansion. Figures 11 and 18 are histories of the **wellbore** wall movement for the two Gas-Frac calculations. Permanent **wellbore** expansion is computed for the case with yielding (Figure 11); the final **wellbore** radius being approximately 0.25 meters. This is significantly different from the observed field results where very little permanent **wellbore** expansion was observed. The discrepancy is attributed partially to the inadequate models of compaction and yielding, and partially to simulating the three-dimensional event with a one-dimensional analysis. Figure 18 shows the **wellbore** wall position as a function of time for the elastic calculation. Only minimal permanent expansion is computed. The residual expansion seen in Figure 18 is a result of the residual quasi-static pressures at the end of the calculation (see Figure 4).

The crack void distribution at 2.5 milliseconds, as computed using the CAVS tensile fracture model and for the calculation with yielding, is shown in Figure 12. The distribution for the elastic calculation is shown in Figure 19a. Note that because of the compaction in the first case, no cracks develop adjacent to **wellbore** wall (Figures 12a and 12b), and as a result, no gas flow from the **wellbore** is computed. In the elastic case cracking and internal gas pressurization of the cracks is computed adjacent to the **wellbore**. Figure 19b is a profile of internal crack pressure.

The crack distributions for these one-dimensional calculations are shown in Figures 13, 20 and 21. Figure 13 is for the first case, which allows yielding, and Figures 20 and 21 are for the elastic calculation. Notice that in both cases the outside boundary of the plots are the same (3.0 meters). The **borehole** expansion in the first case (Figure 13) is to 0.25 meters and in the second case (Figure 20) is to 0.10 meters.

The computed radial crack distributions do not match the observed field results in an absolute sense. In a relative sense however, when comparison is made between the computed crack distributions of the other tests considered in this report, the cracking computed is moderately good. **Mineback** observations of the Gas-Frac experiment showed that radial and circumferential cracks developed to about 0.5 meters from the center of the hole. A few longer radial cracks developed to a few meters with a predominate radial crack extended to about 6 meters.

2.3 Kinefrac (Single Shot) Experiment

The Kinefrac **wellbore** stimulation treatment developed by Kineteck Corporation (8) is a small diameter (4 cm) pressure-insensitive propellant charge that is designed both to initiate and propagate multiple cracks. The charge is centralized in the **wellbore** and is surrounded by a water buffering fluid. The device is designed to push water into the cracks ahead of the gas generated by the propellant reaction products. A **typical** rise time is about 3 milliseconds with a burn time of about $\frac{1}{2}$ second. Details of the field test set-up and the measured pressures, accelerations and stresses are given in References 12, 13 and 14.

The calculational model and initial conditions used in the simulation of this experiment are shown in Figure 3. The applied **wellbore** wall pressure history is shown in Figure 5. The tuff material properties are summarized on Table 1 and Figures 1 and 2. The **multiple** shot Kinefrac experiment was not considered in these calculations.

The peak cavity pressures achieved in the **wellbore** for the Kinefrac shot were about one-fifth those achieved in the Gas-Frac shot. As such, the

computed near-wellbore yielding is much smaller. The extent of **wellbore** expansion, the computed cracking and void strain distribution and internal crack pressure profiles compare quite favorably with the observed **mineback** results.

Figures 22 through 25 respectively, show the computed radial acceleration, radial stress and tangential stress at the **wellbore** wall, at 1.5 feet from the **wellbore** center, at 3.0 feet from the **wellbore** center, and at 6 feet from the **wellbore** center. **Wellbore** expansion in the shot was observed to be minimal. Figure 26 shows the computed history of the **wellbore** wall position. The computed results follow, in time, the applied pressure pulse and are quite minimal.

Figures 27 through 20 are the results of the CAVS computed fracture description. These results are quite favorable in comparison to observed **mineback** results. The single Kinefrac shot produced radial cracks to 1 to 3 feet. All cracks were tight. Figure 27a shows the computed crack void strain distribution and Figure 27b shows the computed crack internal pressurization profile. Note that the crack void strains and the extend of the fluid penetration into the induced cracks are minimal. This compares quite well with observed results. The distribution of induced radial cracks is shown in Figures 28 and 19. At the end of the 20 millisecond calculation the longest crack extends to above 0.3 meter, which also compares quite favorably with observed **mineback** results.

2.4 Dynafrac (Unaugmented) Experiment

The Dynafrac **wellbore** stimulation treatment developed by Physics International (11) is one of the first tailored-pulse concepts investigated. A conventional explosive is used, but the charge diameter is some eight times less than the **wellbore** diameter. The decoupled explosive charge is surrounded by water which mitigates the peak pressure reaching the rock to a value below that which will cause yielding. The total energy release is limited by the small diameter of the charge. The decoupled explosive is designed to initiate multiple cracks and force water into the induced cracks to assist in their extension. Details of the field test set-up and data records are given in References 12, 13 and 14.

The calculational model and initial conditions used in the simulation of Dynafrac experiment are as shown in Figure 3. The applied **wellbore** wall pressure history is shown in Figure 6. The tuff material description is summarized on Table 1 and Figures 1 and 2. The augmented Dynafrac experiment did not function as planned and was not addressed in this evaluation.

Radial acceleration, radial stress and tangential stress histories at the **wellbore** wall, at 1.5 feet from the **wellbore** center, at 3.0 feet from the wellbore, and at 6.0 feet from the **wellbore** center are shown in Figures 30 through 33.

The unaugmented Dynafrac shot did not produce any significant crack development (radially or circumferentially). However, the **wellbore** was enlarged by 15 - 35 percent due to yielding of the tuff. The computed **wellbore** expansion is shown in Figure 34 and is about an order-of-magnitude less than the observed results. The extent of the crack void strain, internal crack pressurization, and radial crack development compares quite favorably with the observed results. Computed crack void strain is minimal (Figure 35a and 36a) and computed fluid penetration from the **wellbore** is also minimal (Figure 35b and 36b). The CAVS computed radial fracture distribution is shown in Figure 37. Cracking is very minimal extending only to about 6 inches into the tuff.

3. SUMMARY AND CONCLUSIONS

In support of METC's continuing evaluation of the tailored-pulse-loading concept of **wellbore** stimulation, five full-scale experiments have been performed under *in situ* conditions to evaluate five different tailored-pulse concepts in initiating and propagating multiple fractures from a wellbore. Five horizontal boreholes were drilled into a thick ash-fall tuff formation from a tunnel in Rainier Mesa under 430 meters of overburden. Each **borehole** was fielded with different TPL well stimulation treatments. The five concepts investigated involved:

- a) a small-diameter explosive decoupled with a water pad,
- b) a small-diameter decoupled explosive with water pad and an added propellant booster,
- c) a small-diameter propellant charge with a pressurized water pad,
- d) three successive shots of case c, and
- e) a full-diameter charge of progressively burning propellant.

Each test was executed after pre-test evaluation of the **borehole** condition and permeability. Cavity pressure records were obtained in the **wellbore** for each test. Accelerometer and stressmeter data were also obtained at several locations in the tuff for each test. Post-test evaluation included caliper and TV logs of the wellbore, permeability measurements and **mineback** for direct observation of the induced fracture patterns.

Field record data, material property data of the tuff, and *in situ* initial stresses enabled a computational evaluation to be performed. This evaluation was performed using the STEALTH finite-difference codes and was intended to provide a comparison between observed results and computed results. Of primary concern in the computational investigation was the degree of **wellbore** expansion due to yielding and compaction of the near-borehole rock and the extent of induced fractures. Three of the above mentioned experiments were considered for evaluation; the Gas-Frac experiment (test e), the single Kinefrac experiment (test c), and the unaugmented Dynafrac experiment (test a). The augmented Dynafrac test (test b) failed to perform

as planned and was not considered. The multiple Kinefrac test (test d) was a repetition of the single Kinefrac shot.

Results of the computational evaluation of the three treatments addressed are as follows:

- 1) In all calculations, the computed radial acceleration, radial stress and tangential stress histories at the instrumentation locations were about an order-of-magnitude larger than the field records. The discrepancy is predominantly attributable to the fact that the calculations were one-dimensional descriptions of a three-dimensional event. Also, the material descriptions used to model the water saturated tuff were probably not completely adequate. The material properties were obtained from quasi-static laboratory experiments where drainage of the pore fluid was allowed, in contrast to the dynamic probably undrained conditions of the field tests.
- 2) The Gas-Frac shot produced peak **borehole** pressures of several hundred mega-pascals (an order-of-magnitude larger than the Kinefrac shot and about three times that of the Dynafrac shot). The high peak cavity pressures induced considerable compaction of **the** tuff near the wellbore, as computed in the **numerical** simulation. This compaction was not observed in the field and suggests inappropriate compaction and/or yield models for the tuff, at least at these high stresses. The computed radial fracture development (using the **CAVS** model of tensile failure) was, in an absolute sense, somewhat less **than** the field results, although in a relative sense (when compared to the Kinefrac and Dynafrac simulations) is moderately good. The maximum computed radial crack length was about 1.5 meters. Observed field results indicated concentrated cracks (radial and circumferential) to about 0.5 meter; a few radial radials to about 1.5 meters; and a major crack to about 6 meters.
- 3) The Kinefrac shot produced peak **borehole** pressures of several tens of mega-pascals. Only **minimal** permanent **wellbore expansion** was observed upon mineback. Compute results **compare** quite favorably. The single Kinefrac test produced radial cracks extending to a **maximum** distance of about 1 meter. All cracks were tight. The compute crack void strain (a measure of the crack width) is minimal and in agreement with observed results. The distribution of radial cracks, as computed, is also in good agreement with observed results. The maximum length of computed radial cracks is about 0.3 meter.

- 4) The unaugmented Dynafrac shot did not produce any significant crack development. The wellbore was enlarged by 15 - 35 percent due to yielding of the tuff. The computed wellbore expansion was about an order-of-magnitude less than the observed results. The computed maximum radial fracture extends to about 6 inches with very minimal crack void development or fluid penetration into the cracks. This compares quite well with the observed results.

REFERENCES

1. Atkinson, R.H., "Strength and Deformational Characteristics of Nevada Test Site Tuff," Prepared for Science Applications, Inc., Fort Collins, Colorado by Atkinson-Noland and Associates, Inc., Boulder, Colorado, May 1980.
2. **Barbour**, T.G., "Evaluation of EL836 Explosive Stimulation of Devonian Gas Shale," Task Technical Report under Contract **DE-AT21-78-MC08216** for Morgantown Energy Technology Center, Morgantown, West Virginia. Prepared by Science Applications, Inc., Fort Collins, Colorado, September 1980.
3. **Barbour**, T.G., Maxwell, D.E., and Young, C., "Numerical Model Developments for Stimulation Technologies in the Eastern Gas Shales Project," Task Technical Report under Contract EY-78-C-21-8216 for Morgantown Energy Technology Center, Morgantown, West Virginia. Prepared by Science Applications, Inc., Fort Collins, Colorado, January 1980.
4. **Barbour**, T.G., and Mihalik, G.R., "Parameter Sensitivity Analysis of Tailored-Pulse-Loading Stimulation of Devonian Gas Shale," Task Technical Report under Contract **DE-AT21-78-MC08216** for Morgantown Energy Technology Center, Morgantown, West Virginia. Prepared by Science Applications, Inc., Golden, Colorado, November 1980.
5. **Barbour**, T.G., Wahi, and Maxwell, D.E., "Prediction of Fragmentation using **CAVS**," Society for Experimental Stress Analysis, Fall Meeting, Fort Lauderdale, Florida, October 1980.
6. Blanton, T.L., Young, C., and Patti, N.C., "Material Properties of NTS Tuff for Evaluation of **Mineback** Tests (Draft)," Task Technical Report under Contract **DE-AT21-78MC08216** for Morgantown Energy Technology Center, Morgantown, West Virginia. September, 1980.
7. Butters, S.W., Jones, A.H., and Dropek, R.K., "Material Properties of Nevada Test Site Tuff and Grout - with Emphasis on the Mighty Epic Event," Defense Nuclear Agency DNA 4235F. Prepared by Terra Tek, Inc., November 1976.
8. Fitzgerald, R. and Anderson, R., "Kinefrac - A New Approach to Well Stimulation," **ASME** Paper 78-PET-25, **ASME** Technology Conference and **Exhibition**, Houston, Texas, November 1978.
9. Hofmann, R., "STEALTH, A Lagrange Explicit Finite-Difference Code for Solids, Structural and Thermohydraulic **Analysis**," EPRI NF-176-1, Electric Power Research Institute, Palo Alto, California, Prepared by Science Applications, Inc., San Leandro, California, April 1978.

10. Maxwell, D.E., "The CAVS Tensile Failure Model," SAI Internal Report SATR 79-4. Science Applications, Inc., San Leandro, California April 1979.
11. Moore, E.T., Mumma, D.M., and Seifert, K.D., "Dynafrac - Application of a Novel Rock Fracturing Method in Oil and Gas Recovery," PIFR-827 Physics International, San Leandro, California, April 1977.
12. Schmidt, R.A., Sandia Laboratories, Albuquerque, New Mexico, letter dated September 29, 1980.
13. Schmidt, R.A., Sandia Laboratories, Albuquerque, New Mexico, monthly progress reports. Project - In Situ Testing of Well Shooting Concepts 1979-1980.
14. Schmidt, R.A., Warpinski, W.R., and Cooper, P.W., "In Situ Evaluation of Several Tailored-Pulse Well-Shooting Concepts," Unconventional Gas Recovery Symposium, SPE 8934, Pittsburgh, Pennsylvania, May 1980.
15. Warpinski, N.R., Schmidt, R.A., Walling, H.C., Cooper, P.W., and Finley, S.J., "High Energy Gas-Frac," SAND 78-2342, Sandia Laboratories, Albuquerque, New Mexico, December 1978.

TABLE 1. NTS G-TUNNEL ASH-FALL TUFF MECHANICAL PROPERTIES*

| | | |
|-------------------------------------|--|---|
| <u>DENSITY</u> | | ρ = ρ_o/V , kg/m ³ |
| | | v = relative volume |
| | | ρ_o = initial density, 1800 kg/m ³ |
| <u>ELASTICITY</u> (isotropic) | | |
| Compressibility (equation-of-state) | $0 < \mu \leq 0.01$ | $P = A + B\mu + C\mu^2$, Pa |
| - see Figure 1 | | P = pressure |
| | | $\mu = (1-v) / V$ |
| | | v = relative volume |
| | | $A = 0.0$ Pa |
| | | $B = 3.160 \times 10^8$ Pa |
| | | $C = 3.735 \times 10^{10}$ Pa |
| | $0.01 < \mu \leq 0.0232$ | $P = D + E\mu$, Pa |
| | | $D = 6.895 \times 10^6$ Pa |
| | | $E = 2.09 \times 10^9$ Pa |
| | $0.0232 < \mu$ | $P = F + H\mu$, Pa |
| | | $F = 3.448 \times 10^7$ Pa |
| | | $H = 1.026 \times 10^9$ Pa |
| | unloading/reloading when P is compressive | $P = E\mu$, Pa |
| | | $E = 2.09 \times 10^9$ Pa |
| | unloading/reloading when P is tensile | $P = T\mu$, Pa |
| | | $T = 3.160 \times 10^8$ Pa |
| Distortion (constant shear modulus) | | $G = 1.72 \times 10^9$ Pa |
| <u>PLASTICITY</u> (isotropic) | | |
| Yield Stress (Y) | $P \leq 0$ | $Y = 0.0$ Pa |
| -See Figure 2 | $0.0 < P \leq 1.01 \times 10^8$ Pa | $Y = A + BP + CP^2$, Pa |
| | | Y = yield stress |
| | | P = mean stress |
| | | $A = 2.0 \times 10^7$ Pa |

TABLE 1. NTS G-TUNNELL ASH-FALL TUFF MECHANICAL PROPERTIES* (Continued)

| | |
|---|---|
| | B = 1.01 |
| | C = -5.0×10^{-9} 1/Pa |
| $1.01 \times 10^8 < P$ | Y = 7.10×10^7 Pa |
| Yield Criterion | von Mises as defined in STEALTH |
| Flow Rule | non-associative Prandtl-Reuss as defined in STEALTH |
| TENSILE FAILURE (isotropic) | |
| Virgin tensile strength | $\sigma_k^t = 1.58 \times 10^6$ Pa |
| CAVS ratio of crack initiation - to - crack propagation strength (constant) | R = 2.0 |
| CAVS crack initiation and propagation strengths adjusted according to the degree of nearby cracking | $\sigma_k^t = \sigma_k^t (S^{N_k})$ |
| | $\sigma_k^c =$ current crack initiation strength of three orthogonal cracks (k = 1,2,3), Pa |
| | S = 1.05 (constant) |
| | $N_k =$ number of zone through cracks |
| Tensile Bulk Modulus (constant) | T = 3.160×10^8 Pa |
| CAVS Crack Propping Bulking | B = 10% |
| CAVS Crack Internal Pressurization | not allowed |

TABLE 1. NTS G-TUNNELL ASH-FALL TUFF MECHANICAL PROPERTIES* (Continued)

IN SITU STRESSES (initial, anisotropic)

Borehole Axial Plane

$$\sigma_z = 5.40 \times 10^6 \text{ Pa}$$

Borehole Radial Plane

$$\sigma_x = \sigma_y = 9.45 \times 10^6 \text{ Pa}$$

INITIAL JOINTS (simulating bedding planes)

No

*Compiled from Reference

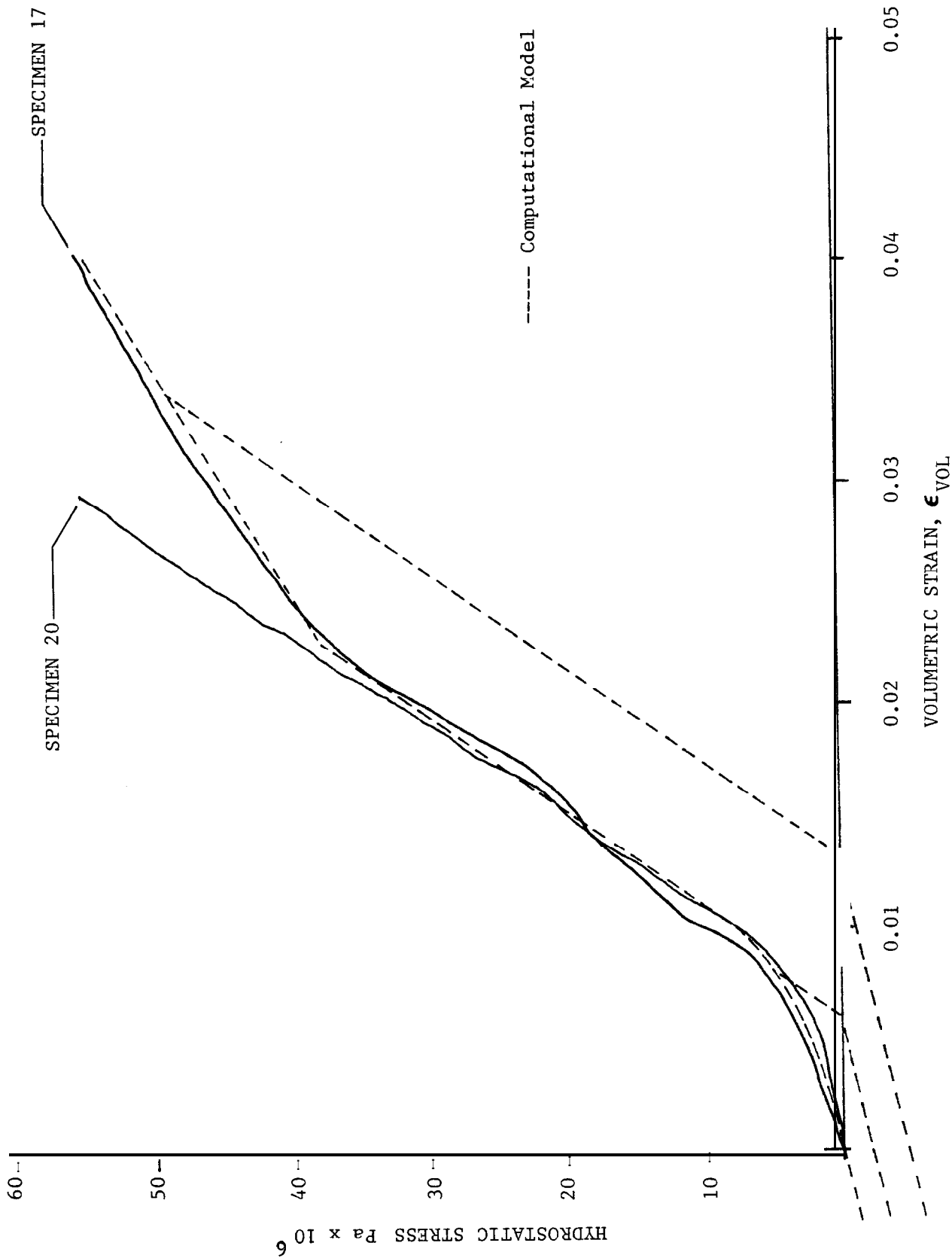


FIGURE 1. G-Tunnel Ash-Fall Tuff Compaction Model

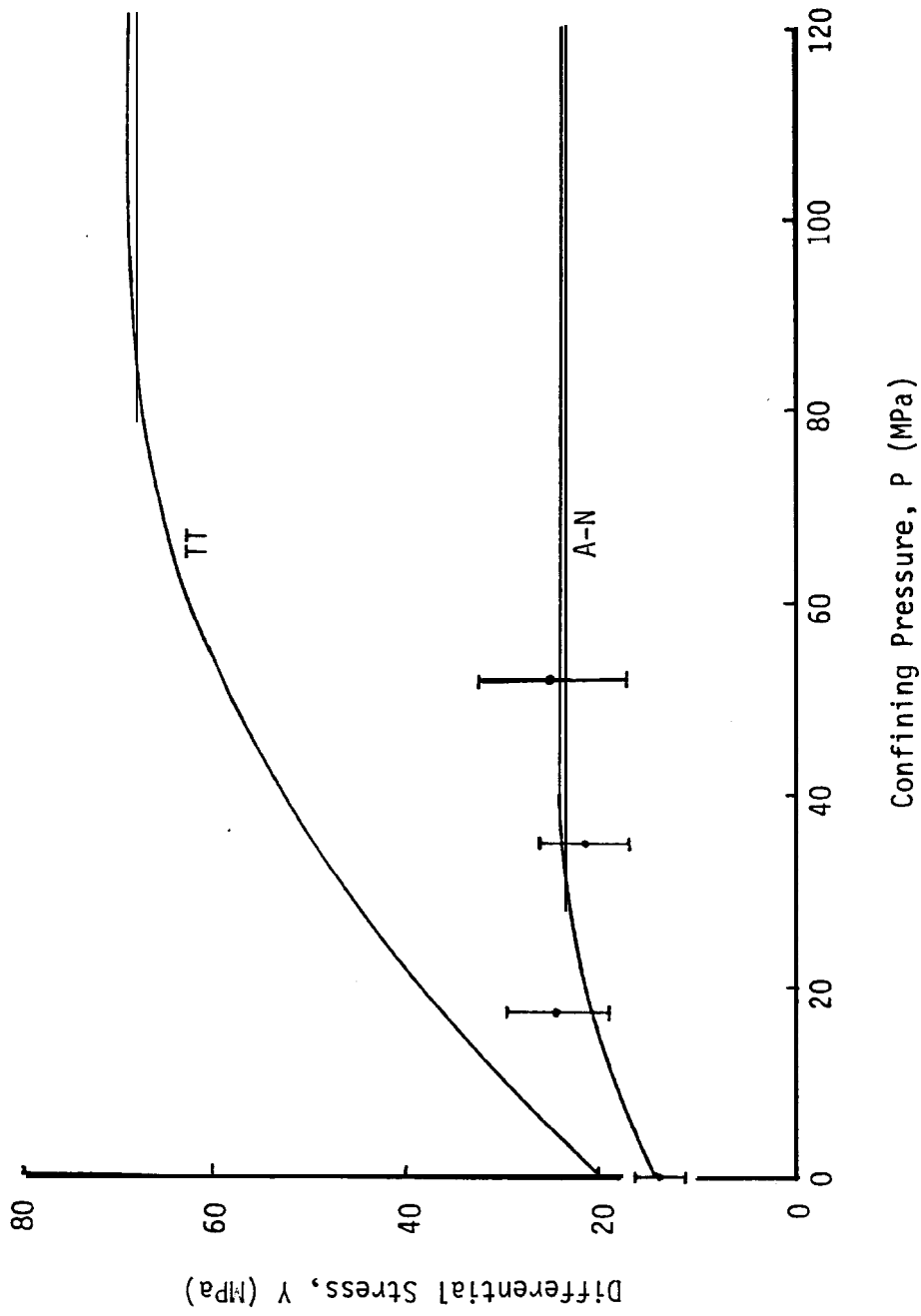
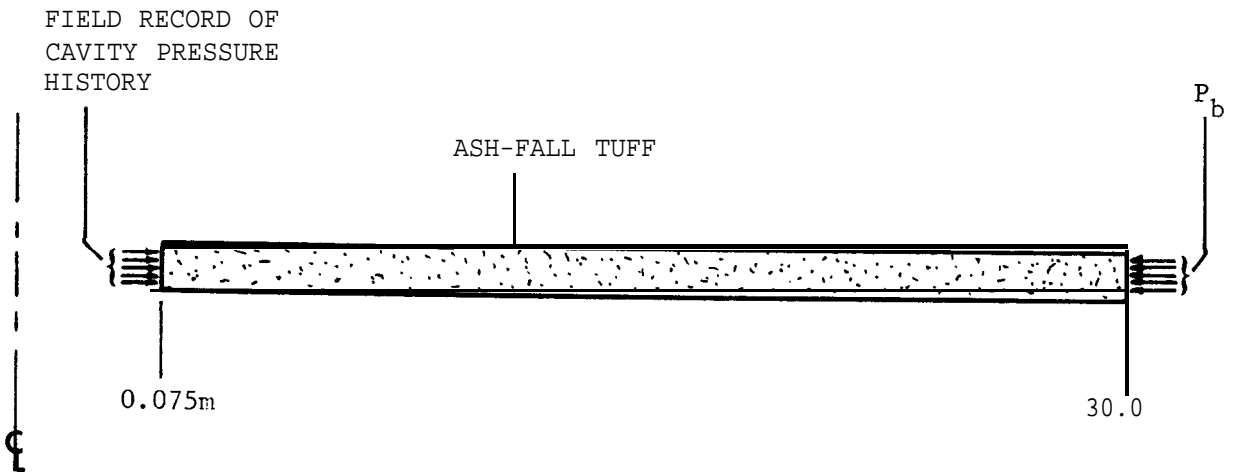


Figure 2. Yield envelopes for NTS ash-fall tuff based on tests run by Atkinson-Noiland (A-N) and Terra Tek (TT).



ZONING

INITIAL CONDITIONS

Tuff

51 Zones (geometric
ratio = 1.075, from
0.075 to 10.0m)

25 Zones (equal,
from 10.0 to 30.0m)

σ_z (tuff), borehole
axial plane -5.40×10^6 Pa

σ_x and σ_y (tuff),
borehole radial plane -9.45×10^6 Pa

P_b (constant) 9.45×10^6 Pa

FIGURE 3. One-dimensional Calculational Model (Geometry and Initial Conditions) for NTS Multi-Frac Experiments

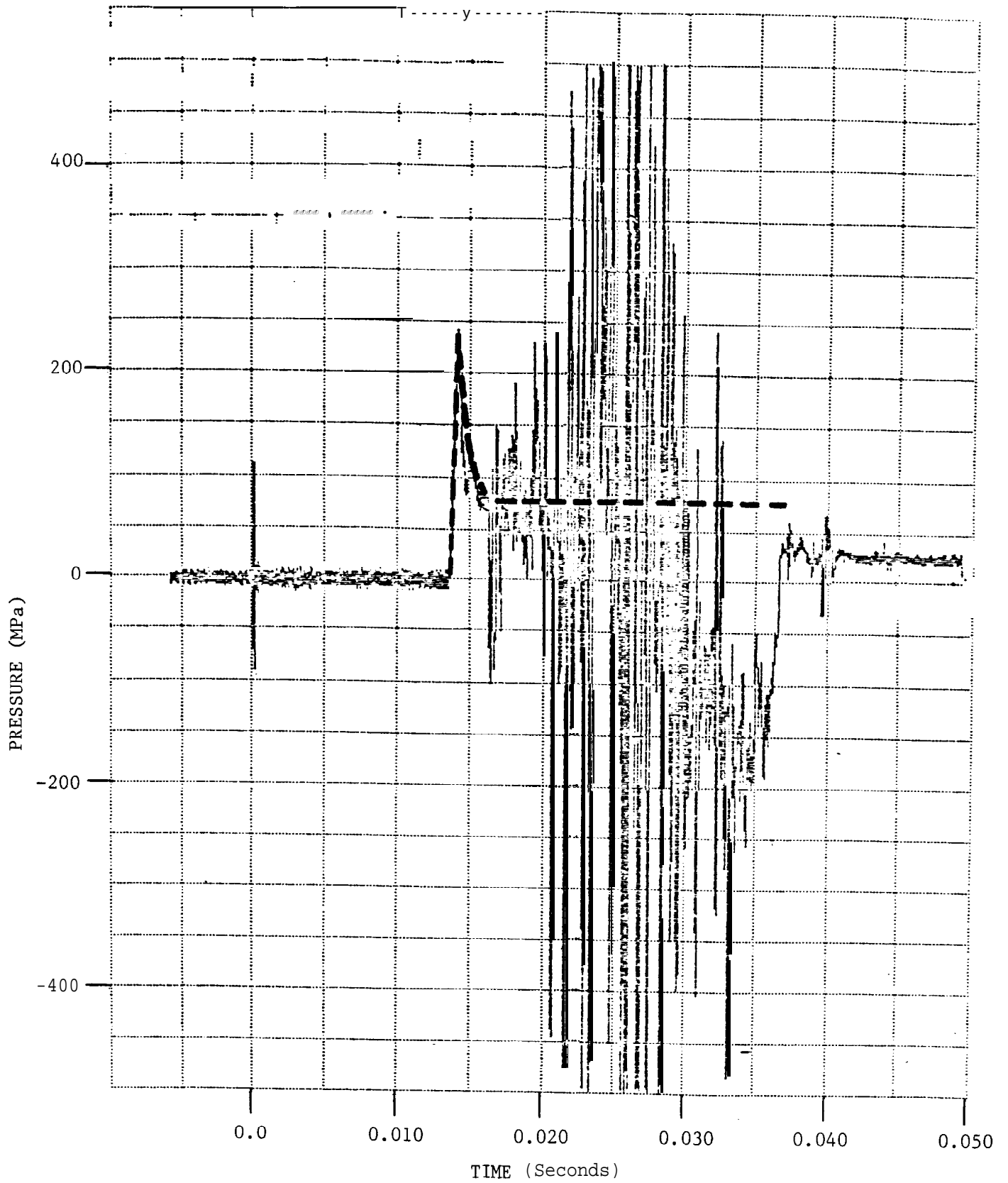


FIGURE 4. Gas-Frac (GF-4) Cavity Pressure Record and Simulated Pressure Pulse

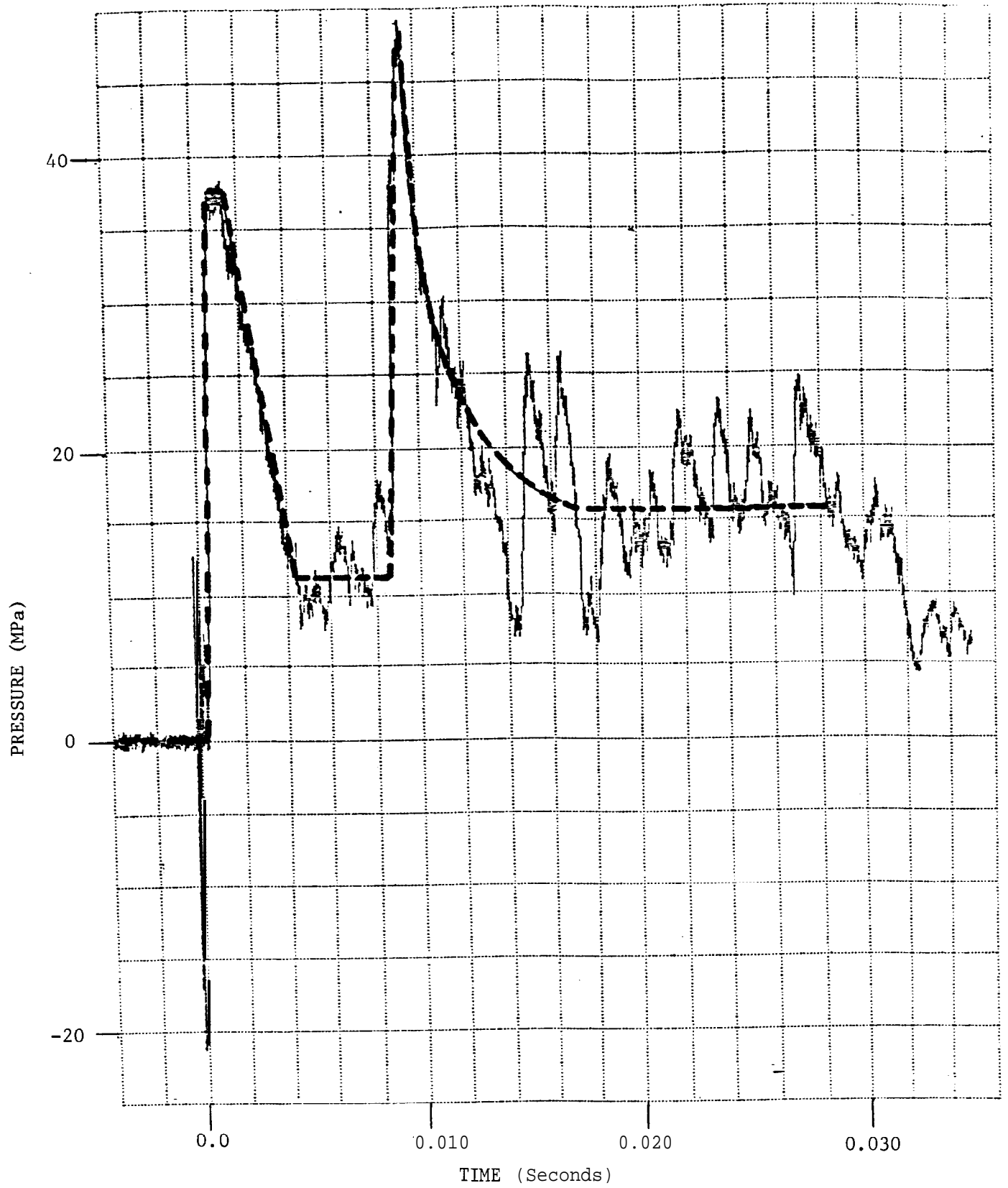


FIGURE 5. Kinefrac (GF-5) Cavity Pressure Record and Simulated Pressure Pulse

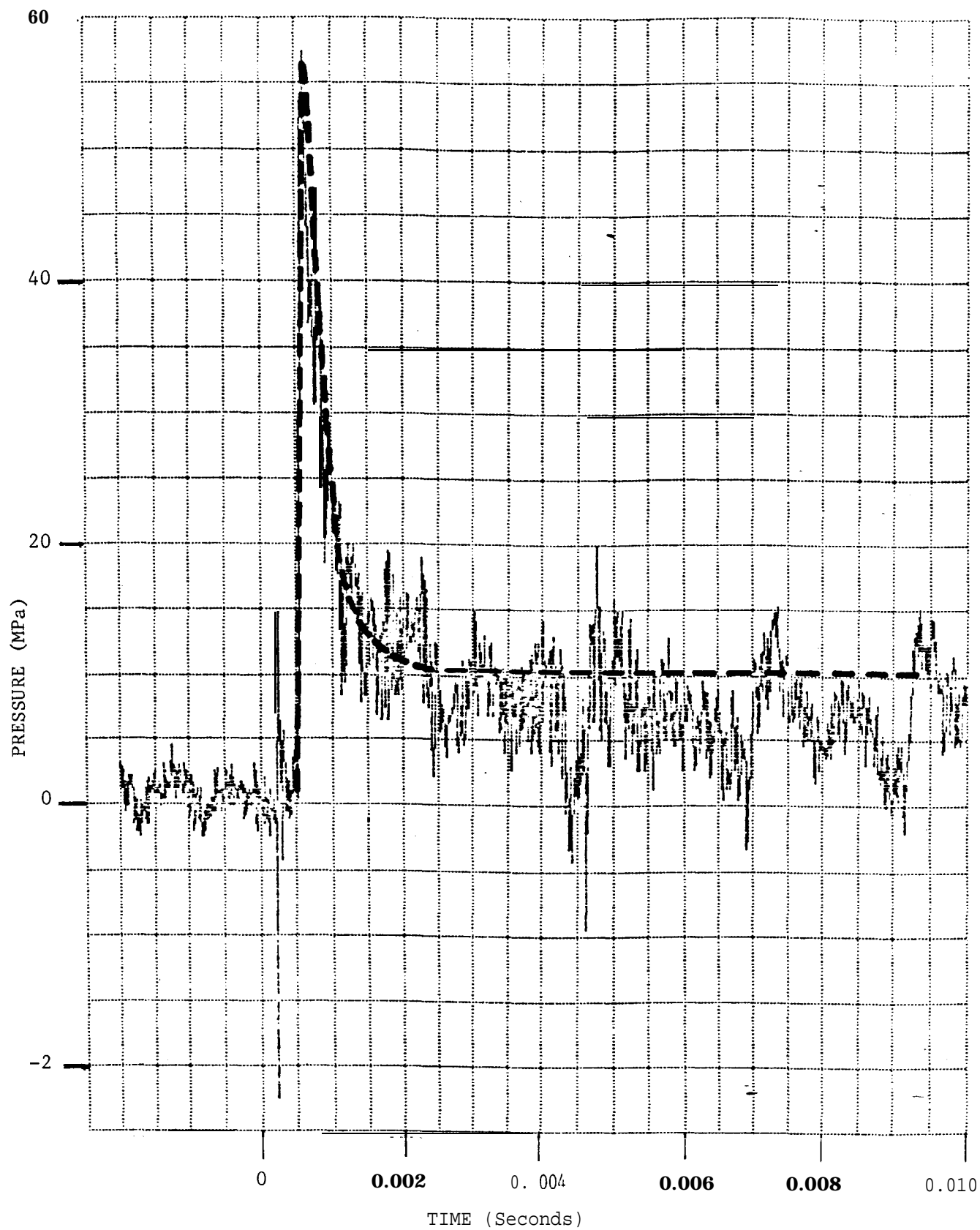


FIGURE 6. Dynafrac (GF-7) Cavity Pressure Record and Simulated Pressure Pulse

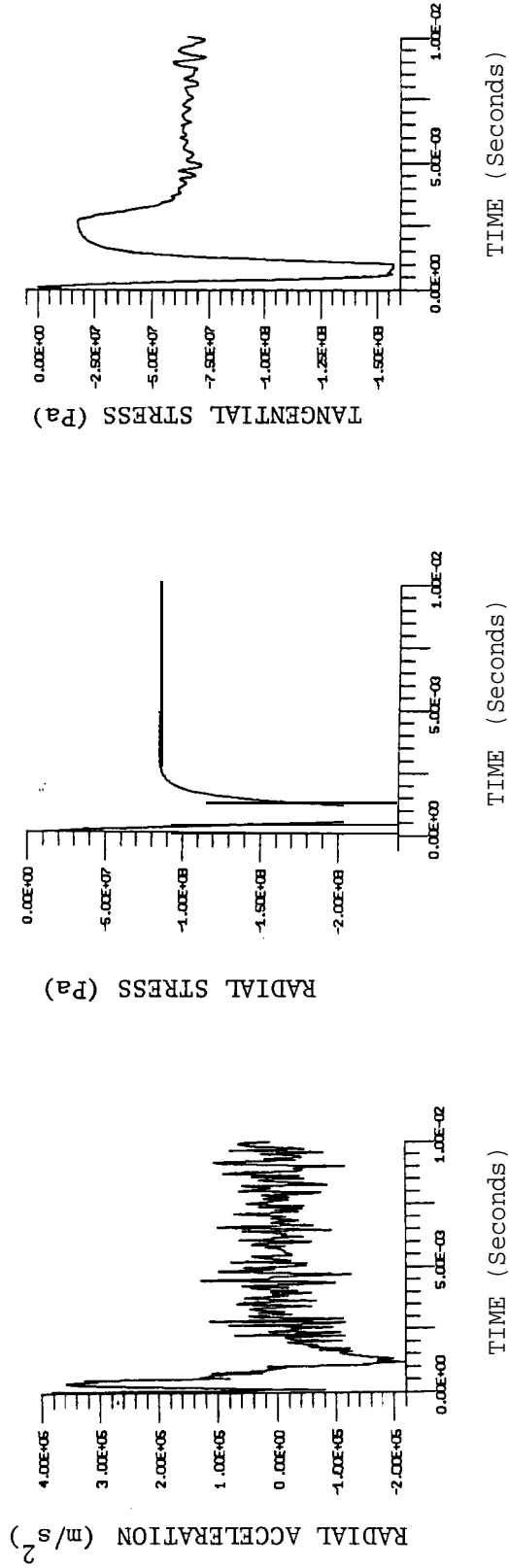


FIGURE 7. Gas-Frac - Radial Acceleration, Radial Stress and Tangential Stress at Wellbore Wall (with tuff compaction and yielding)

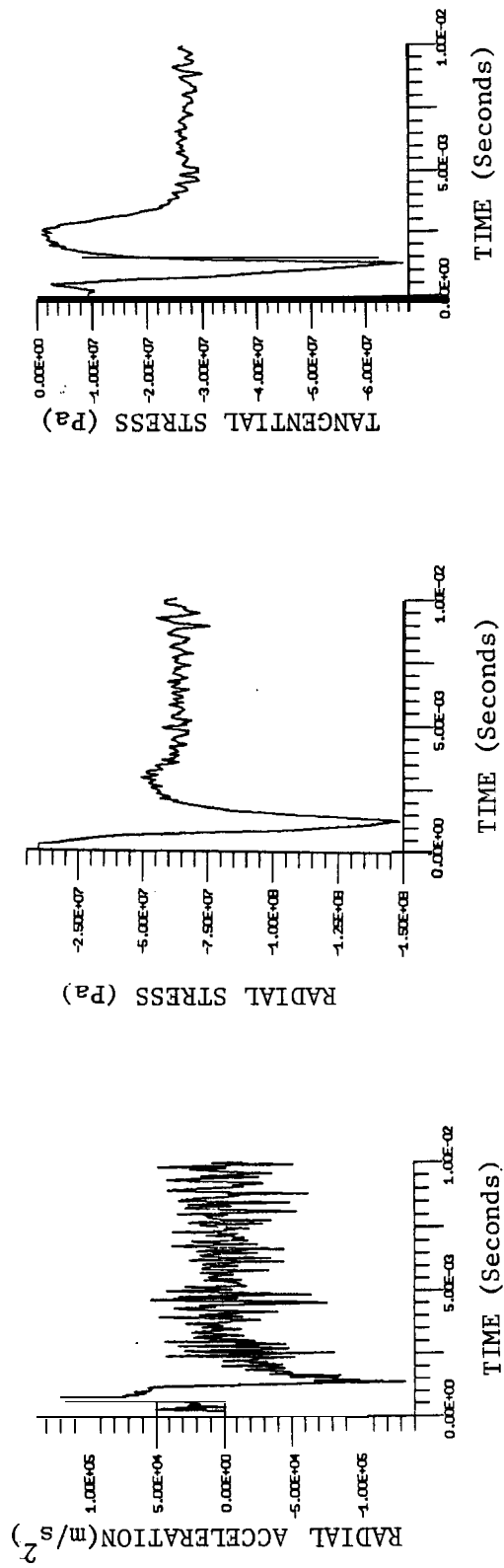


FIGURE 8. Gas-Frac - Radial Acceleration, Radial Stress and Tangential Stress at Approximately 1.5 Feet from Wellbore Center (with tuff compaction and yielding)

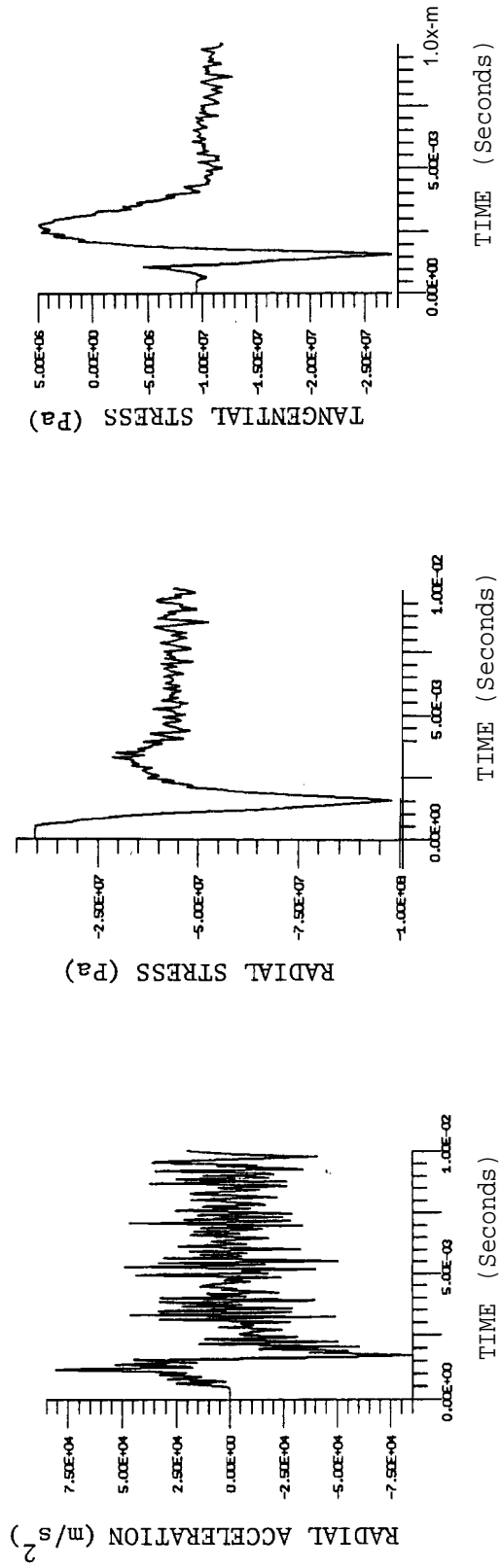


FIGURE 9. Gas-Frac - Radial Acceleration, Radial Stress and Tangential Stress at Approximately 3.0 Feet from Wellbore Center (with tuff compaction and yielding)

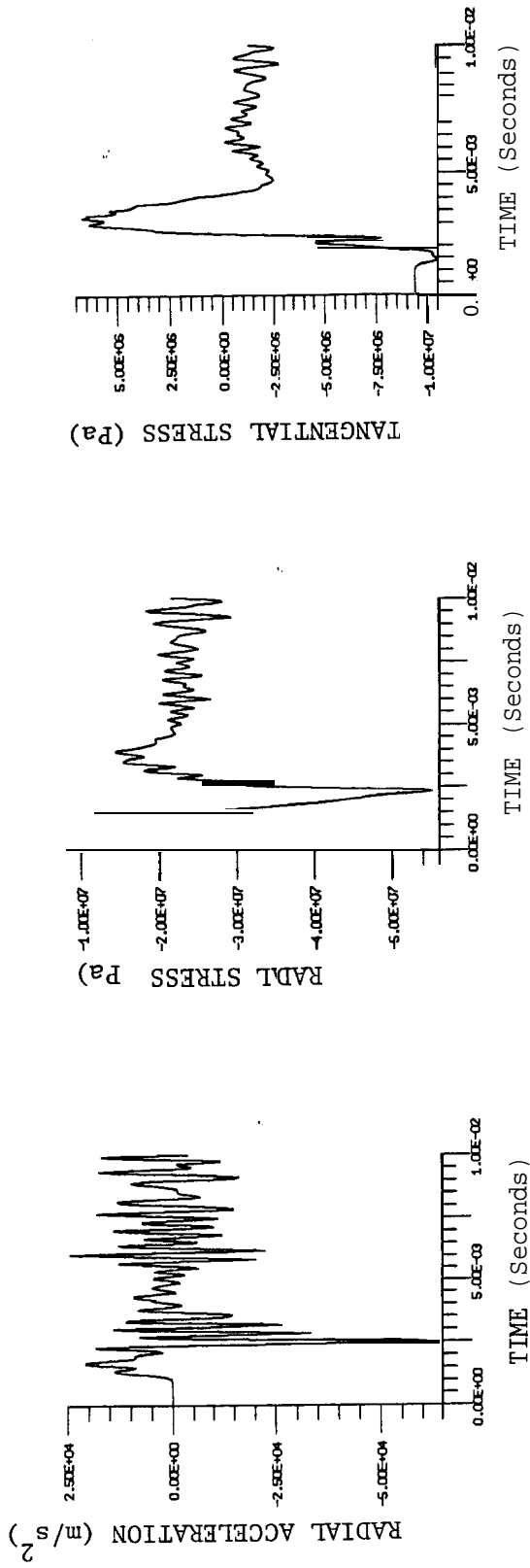


FIGURE 10. Gas-Frac - Radial Acceleration, Radial Stress and Tangential Stress at Approximately 6.0 Feet from Wellbore Center (with tuff compaction and yielding)

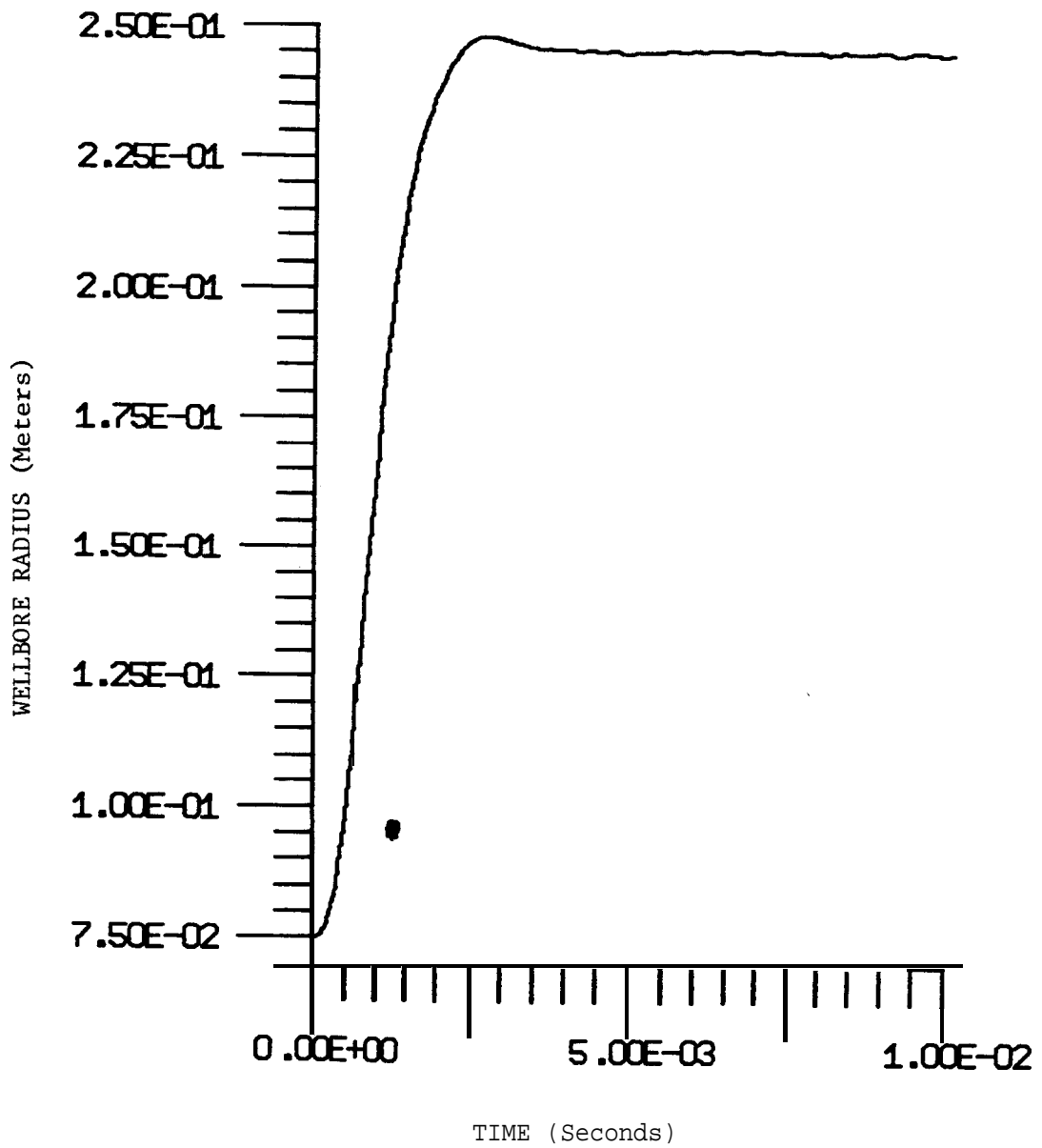


FIGURE 11. Gas-Frac - Wellbore Expansion (with tuff compaction and yielding)

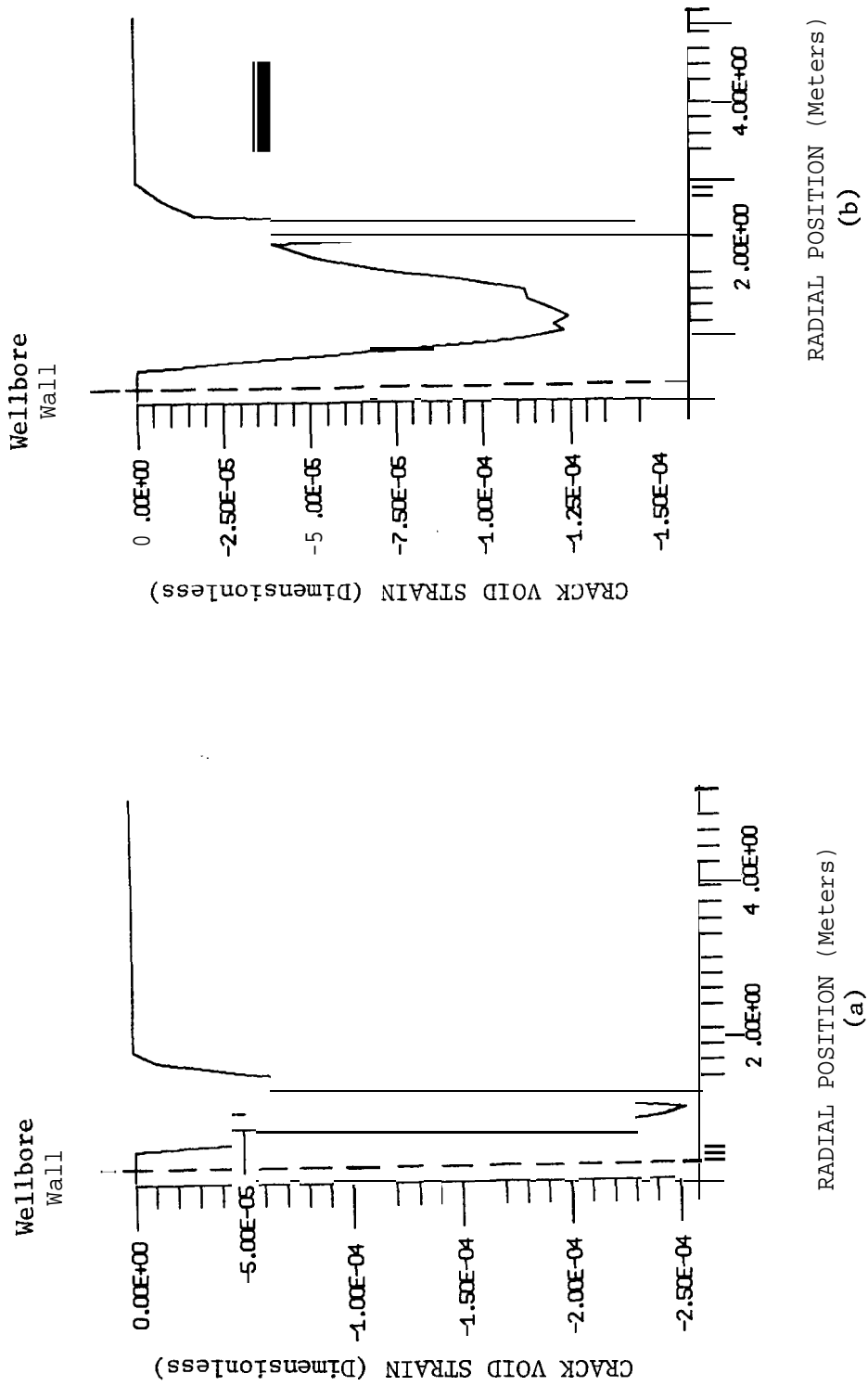
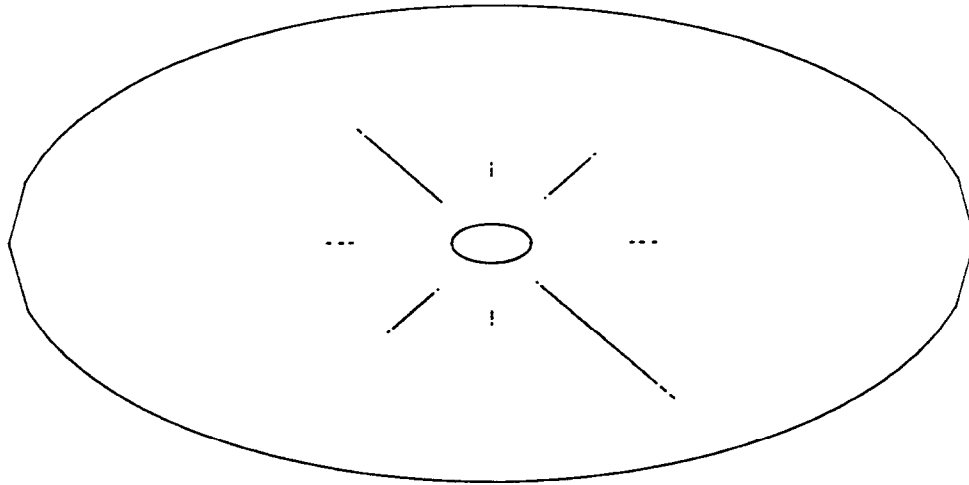
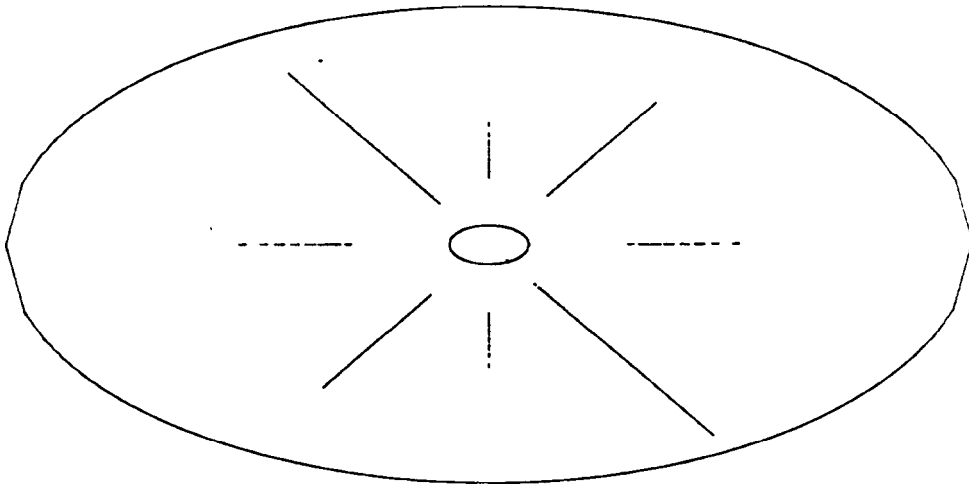


FIGURE 12. Gas-Frac - Crack Void Strain Distribution at 2.5 and 10 Milliseconds (with tuff compaction nad yielding)



Borehole Radius = 0.25 meters
 Outside Boundary = 3.0 meters

a) Radial Cracks at 3 Milliseconds



Borehole Radius = 0.25 meters
 Outside Boundary = 3.0 meters

b) Radial Cracks at 5 Milliseconds

(no additional computed cracking after 5 milliseconds)

FIGURE 13. Gas-Frac - CAVS Fracture Plot at 3 and 5 Milliseconds (with tuff compaction and yielding)

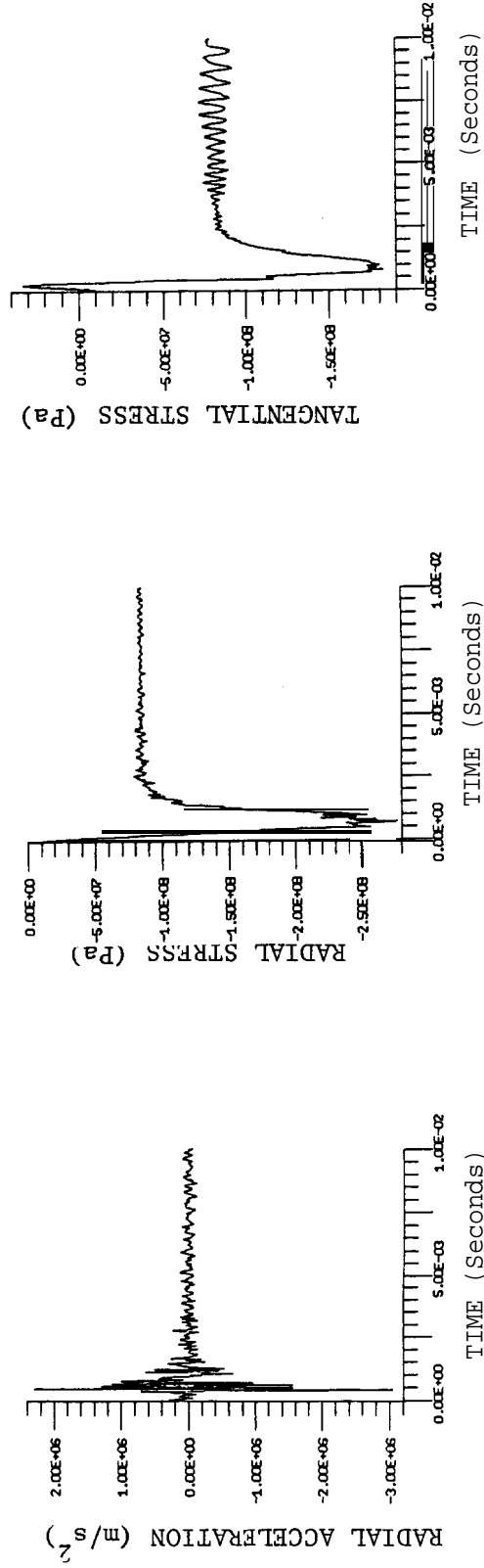


FIGURE 14. Gas-Frac - Radial Acceleration, Radial Stress and Tangential Stress at Wellbore Wall (without tuff compaction or yielding)

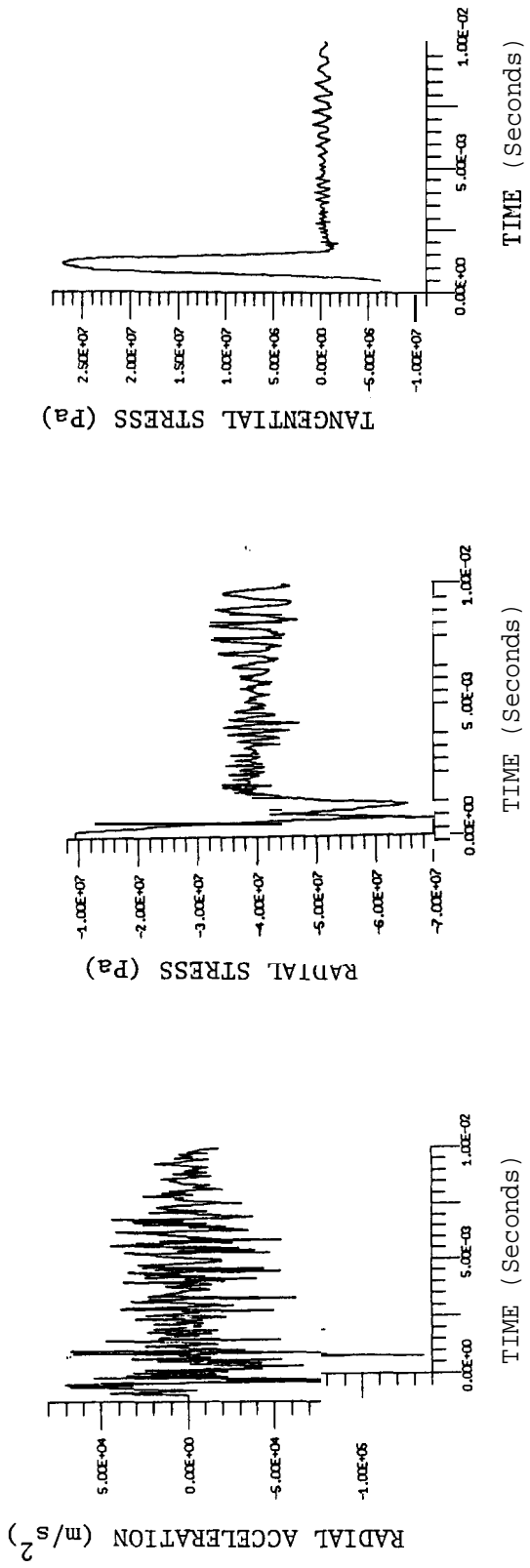


FIGURE 15. Gas-Frac - Radial Acceleration, Radial Stress and Tangential Stress at Approximately 1.5 Feet from Wellbore Center (without tuff compaction or yielding)

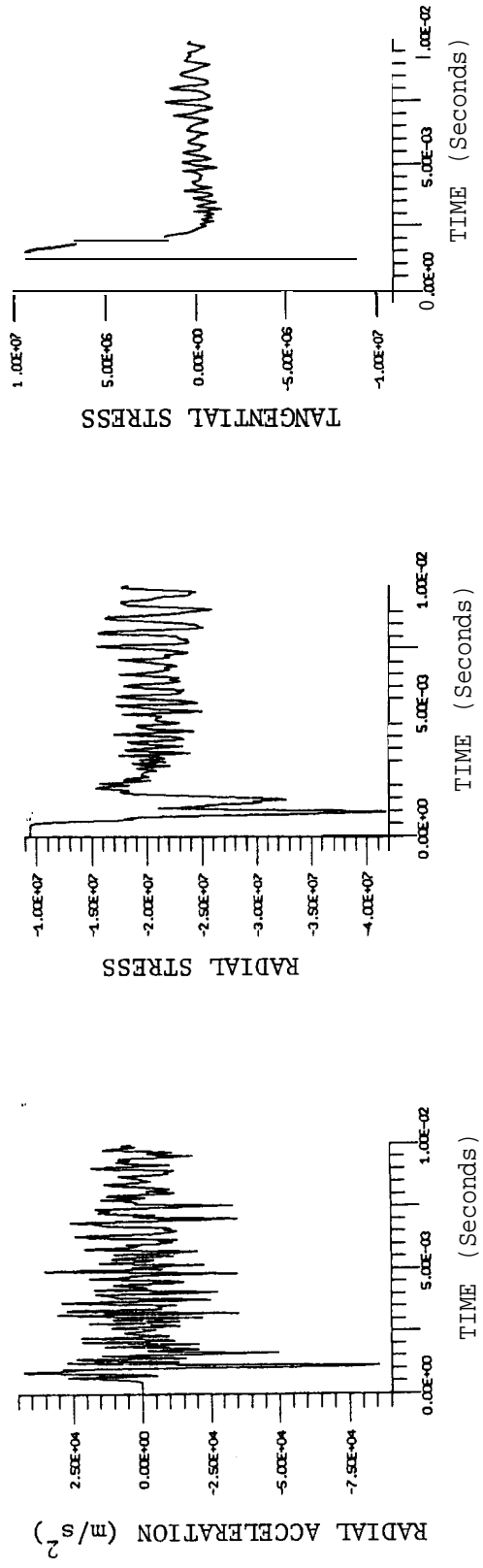


FIGURE 16. Gas-Frac - Radial Acceleration, Radial Stress and Tangential Stress at Approximately 3.0 Feet from Wellbore Center (without tuff compaction or yielding)

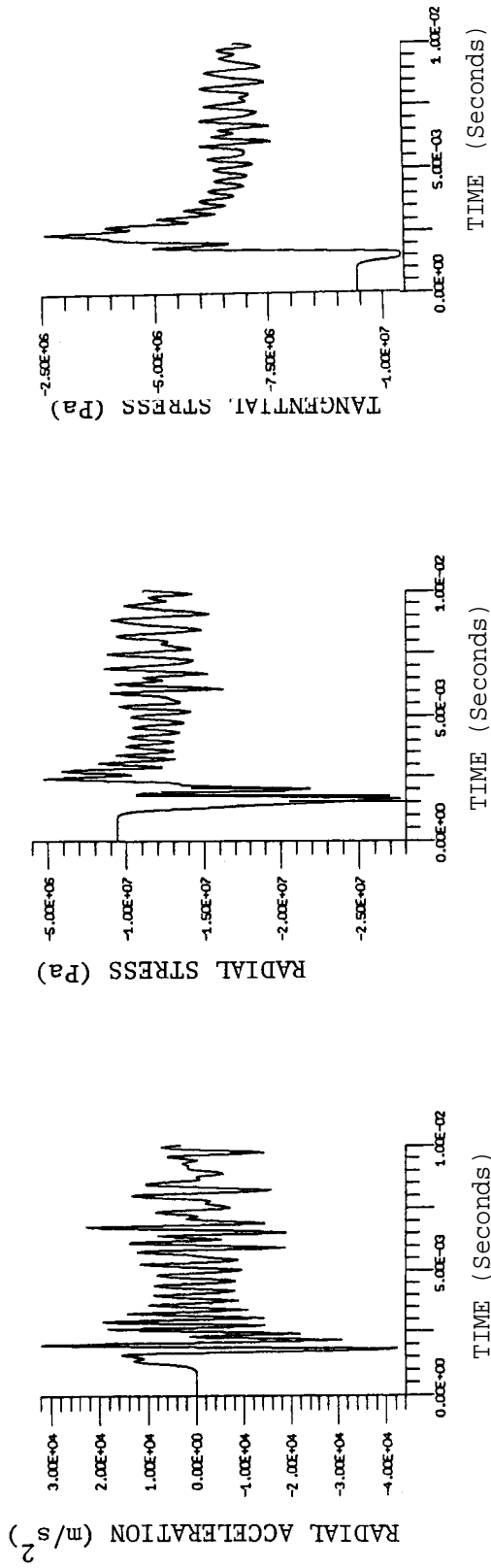


FIGURE 17. Gas-Frac - Radial Acceleration, Radial Stress and Tangential Stress at Approximately 6.0 Feet from Wellbore Center (without tuff compaction or yielding)

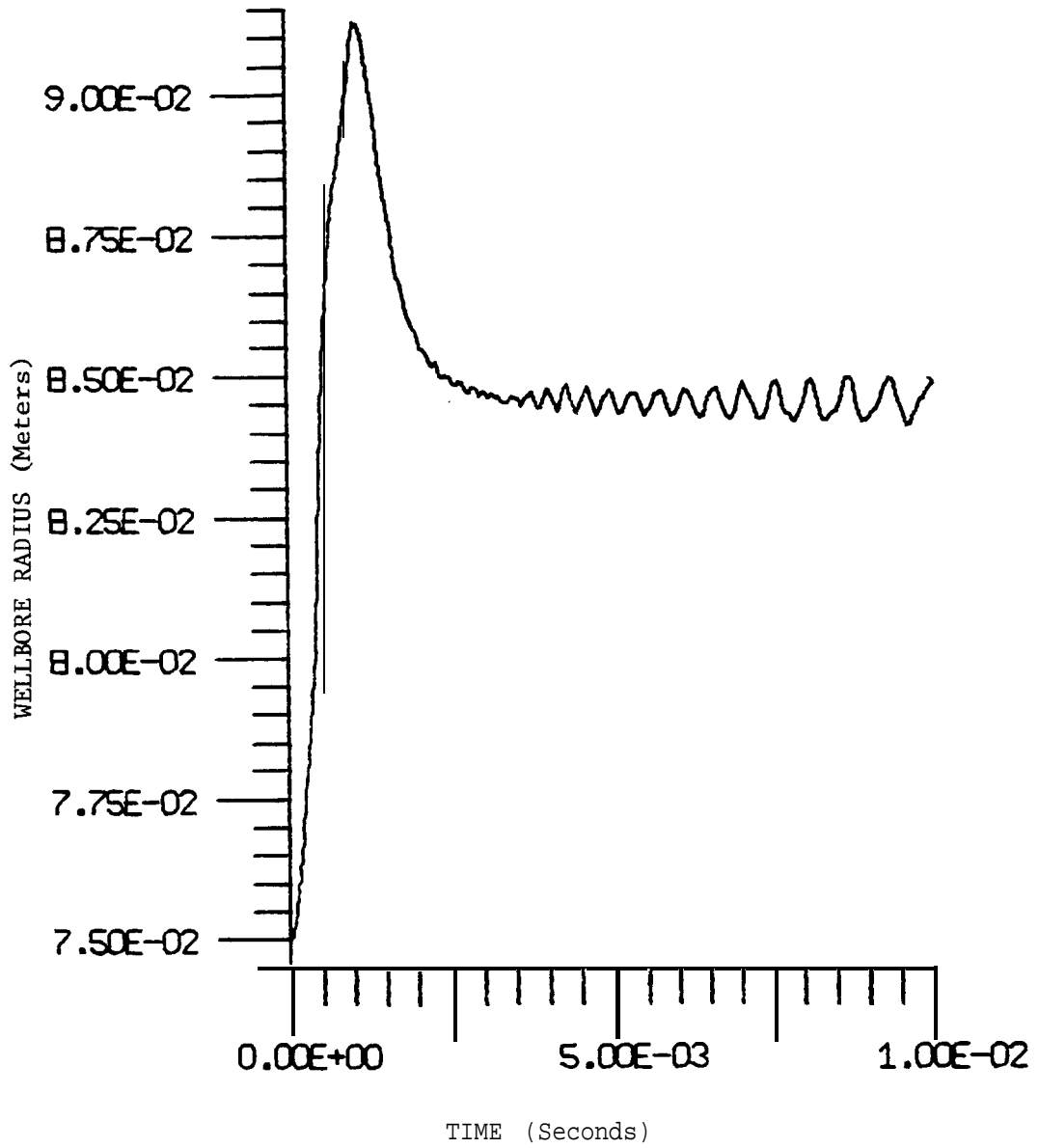


FIGURE 18. Gas-Frac - Wellbore Expansion (without tuff compaction or yielding)

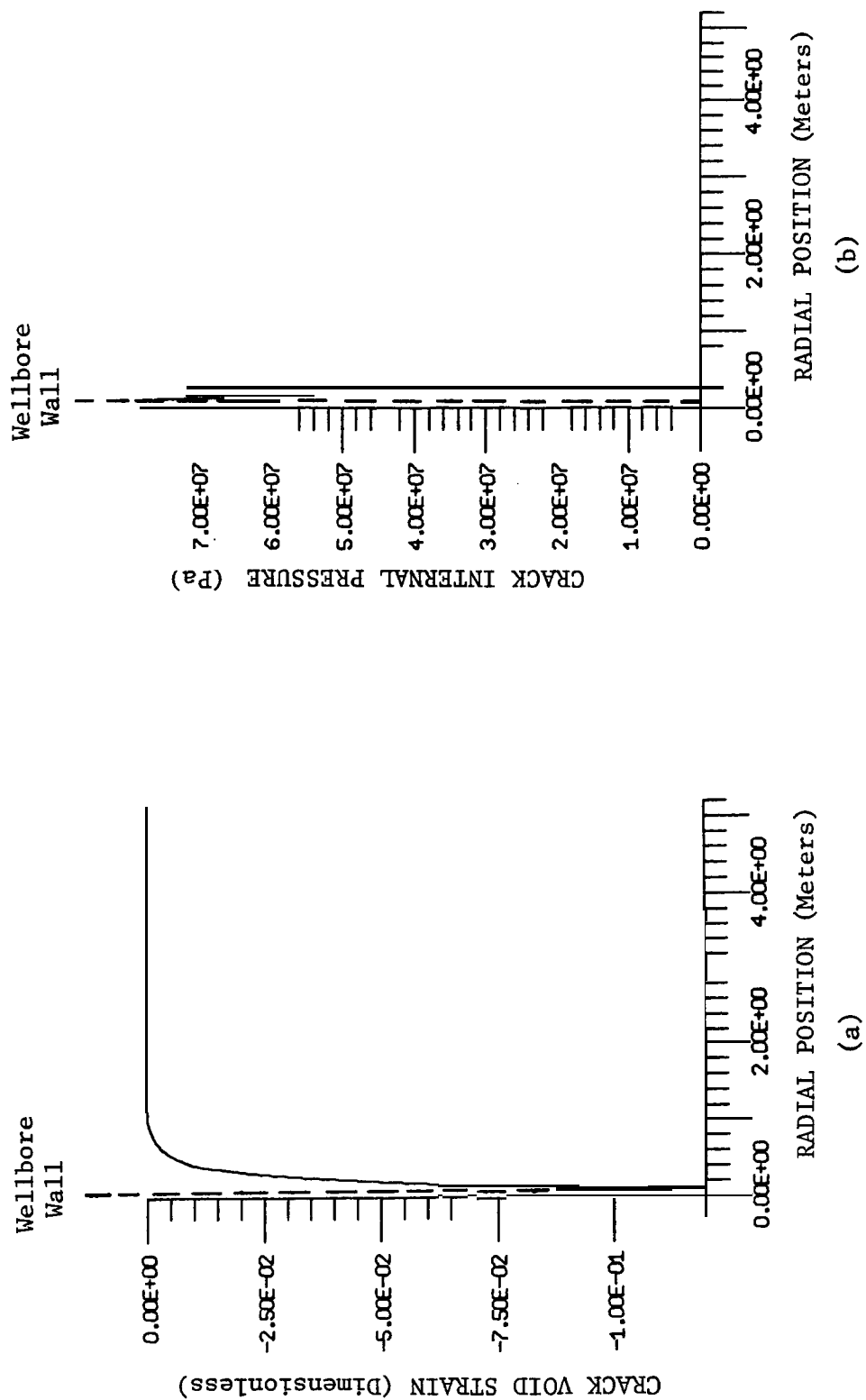
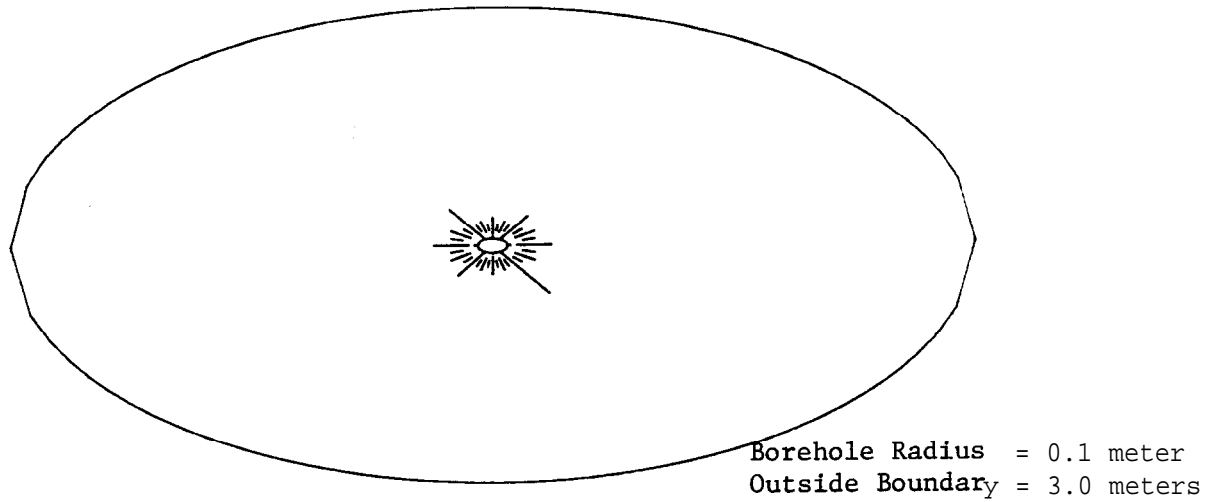
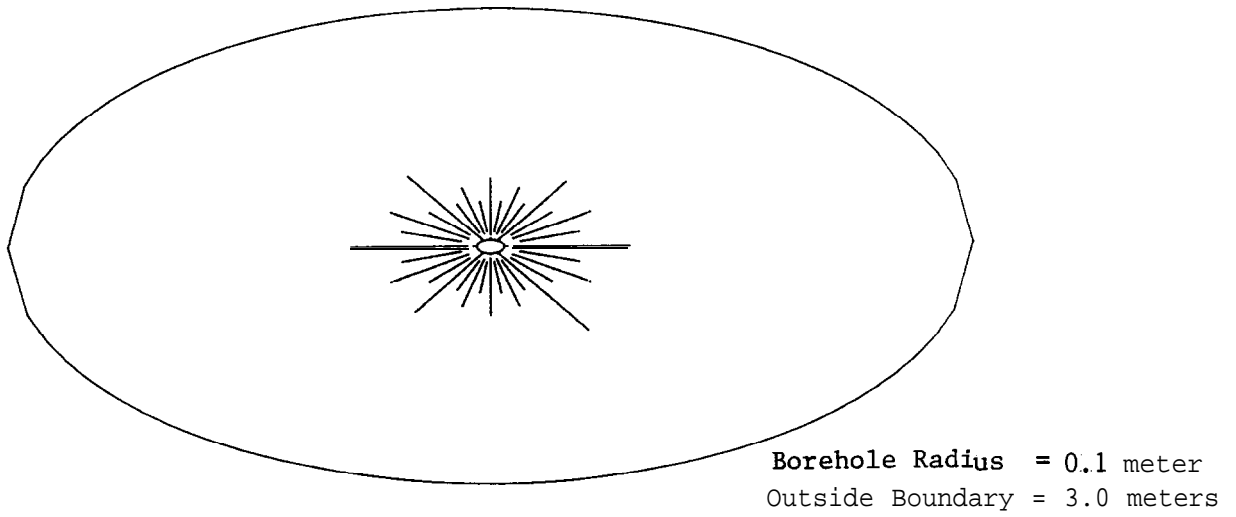


FIGURE 19. Gas-Frac - Crack Void Strain Distribution and Crack Internal Pressure Profile at 10 Milliseconds (without tuff compaction or yielding)

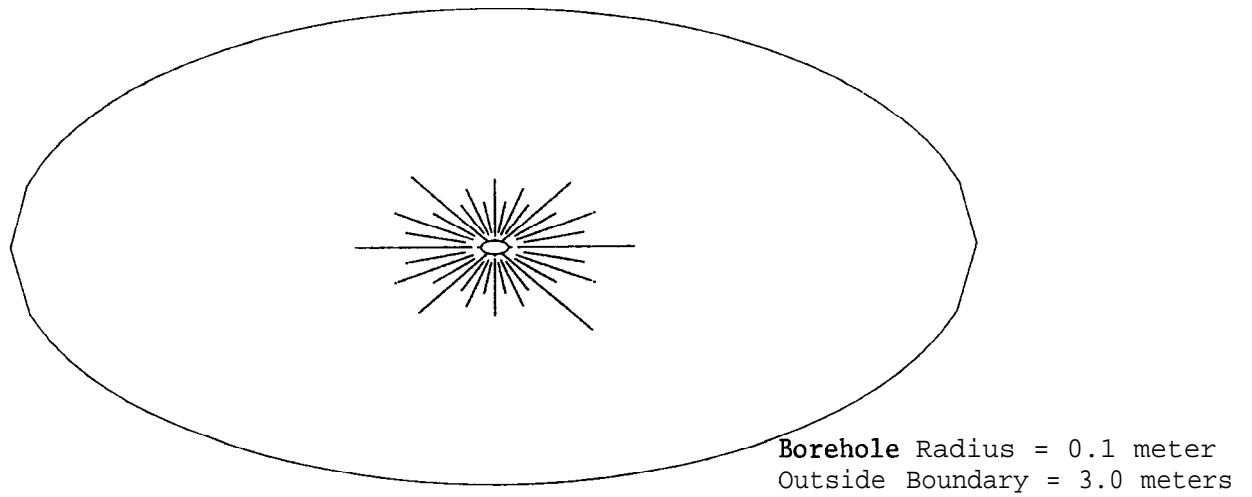


a) Radial Cracks at 1 Millisecond

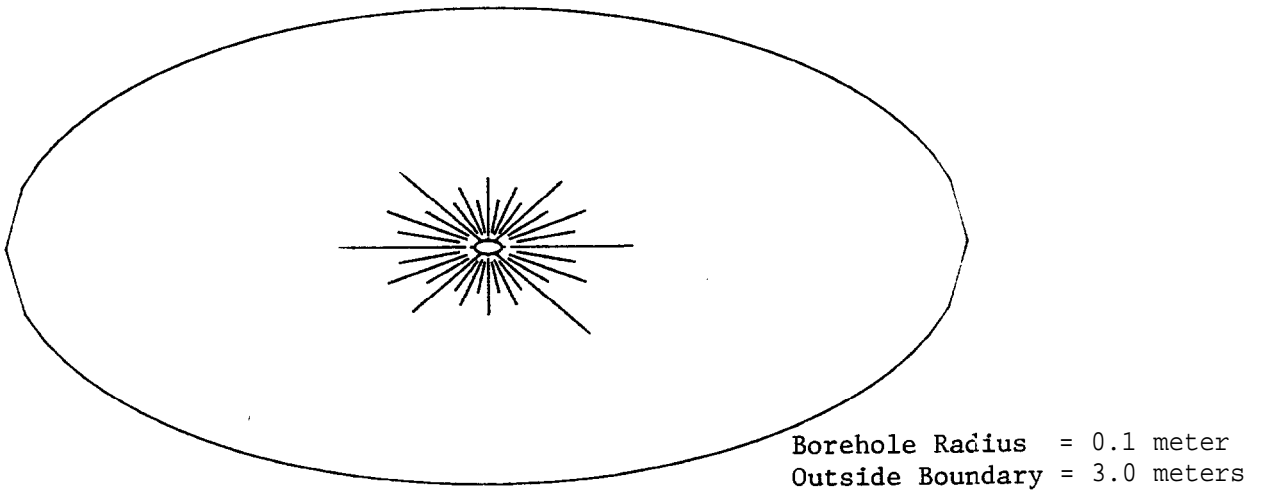


b) Radial Cracks at 2 Milliseconds

FIGURE 20. Gas-Frac - CAVS Fracture Plot at 1 and 2 Milliseconds (without tuff compaction or yielding)



a) Radial Cracks at 3 Milliseconds



b) Radial Cracks at 5 Milliseconds

(no additional computed cracking after 5 milliseconds)

FIGURE 21. Gas-Frac - CAVS Fracture Plot at 3 and 5 Milliseconds (without tuff compaction or yielding)

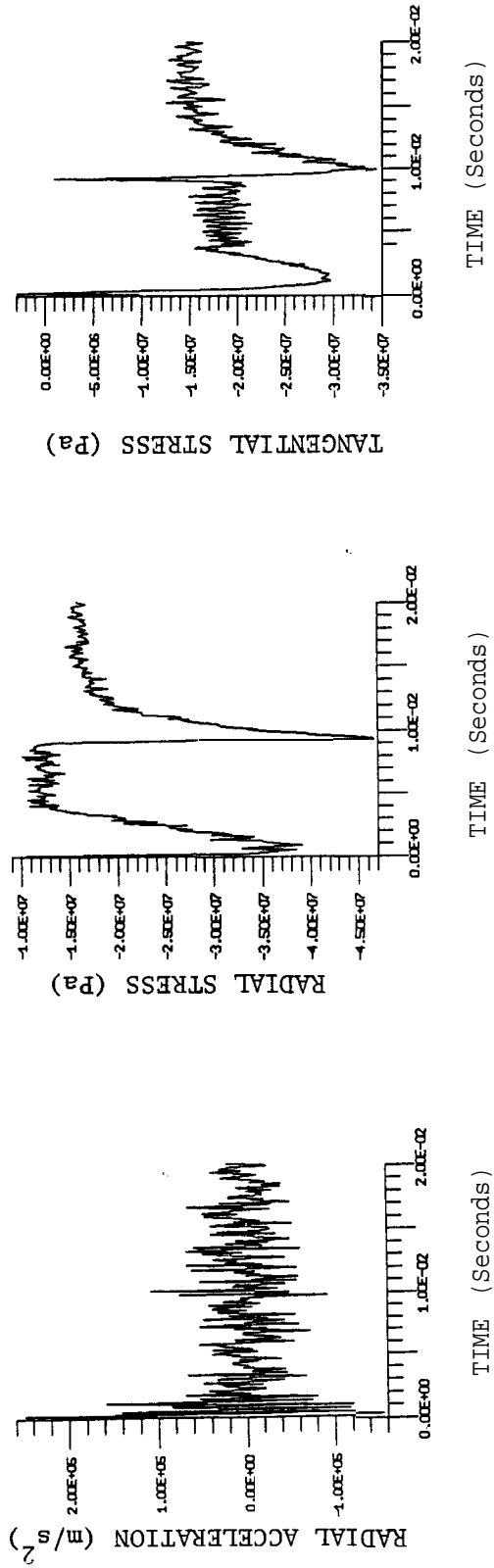


FIGURE 22. Kinefrac - Radial Acceleration, Radial Stress and Tangential Stress at Wellbore Wall

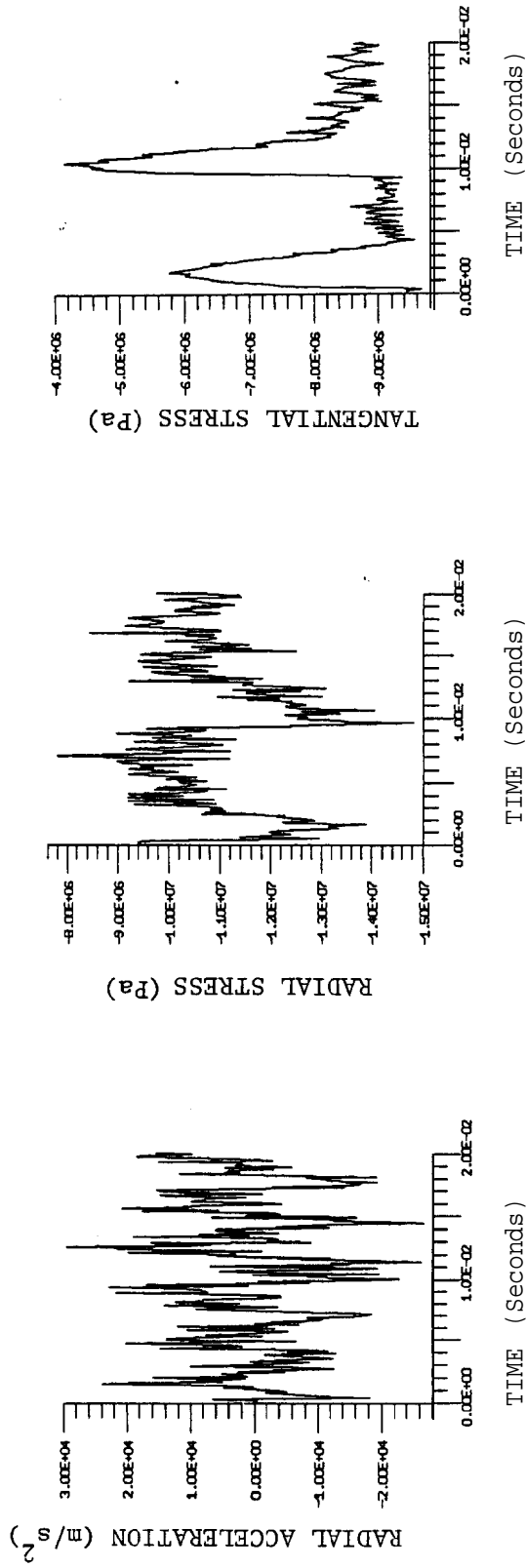


FIGURE 23. Kinefrac - Radial Acceleration, Radial Stress and Tangential Stress at Approximately 1.5 Feet from Wellbore Center

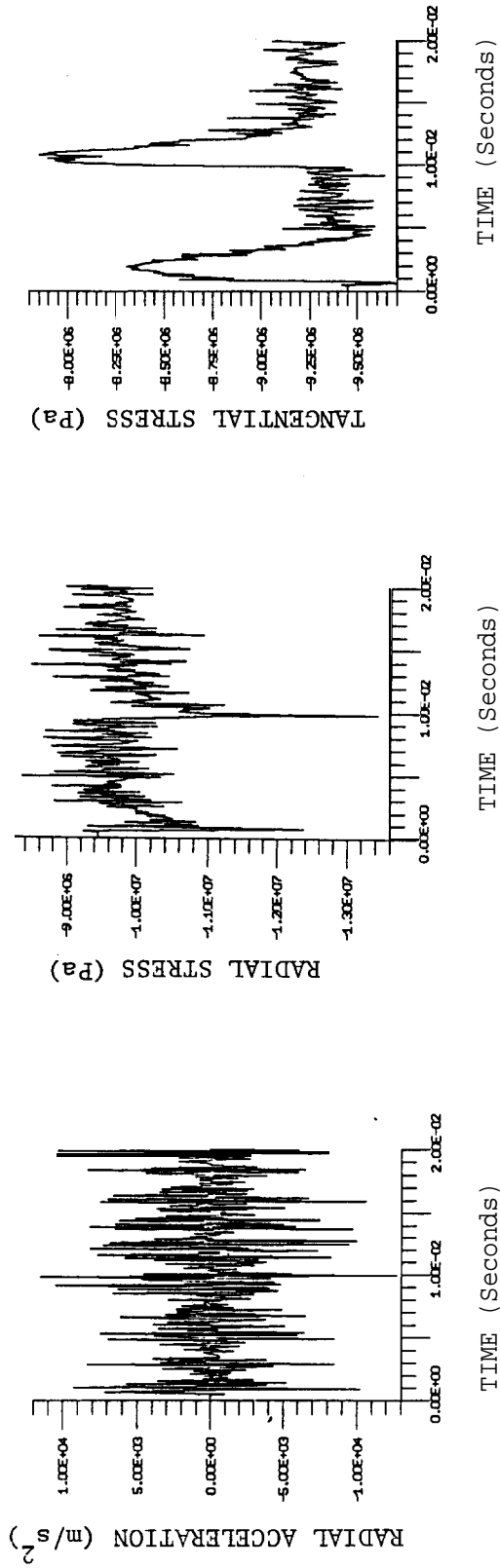


FIGURE 24. Kinefrac - Radial Acceleration, Radial Stress and Tangential Stress at Approximately 3.0 Feet from Wellbore Center

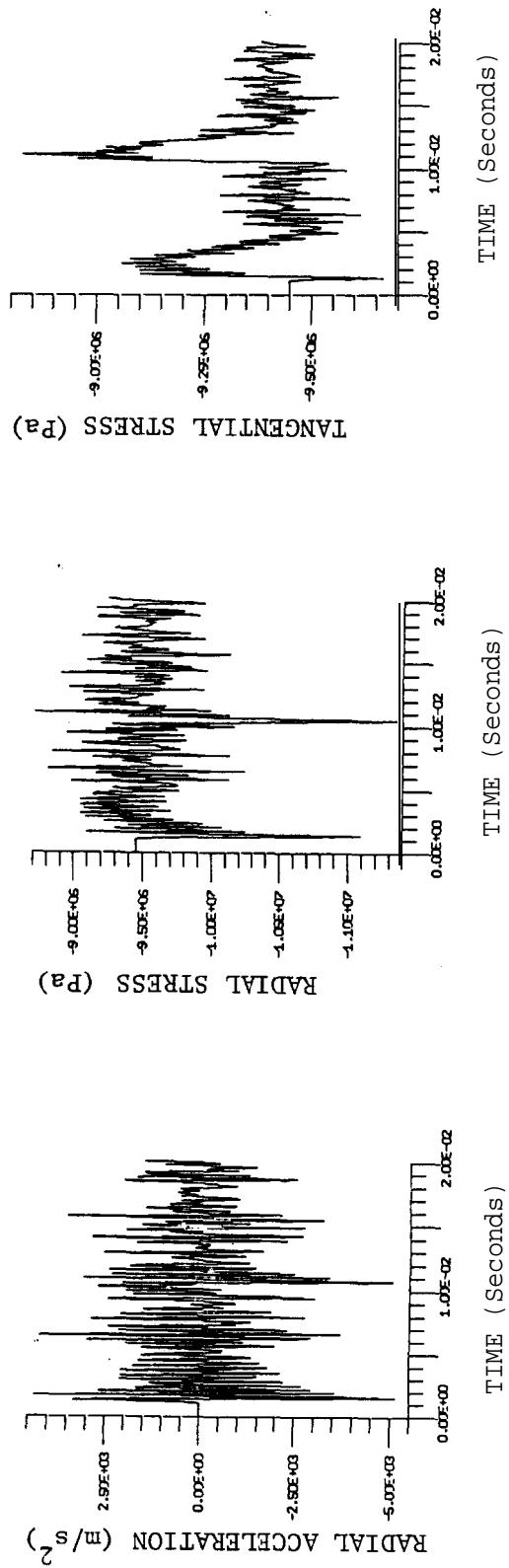


FIGURE 25. Kinefrac - Radial Acceleration, Radial Stress and Tangential Stress at Approximately 6.0 Feet from Wellbore Center

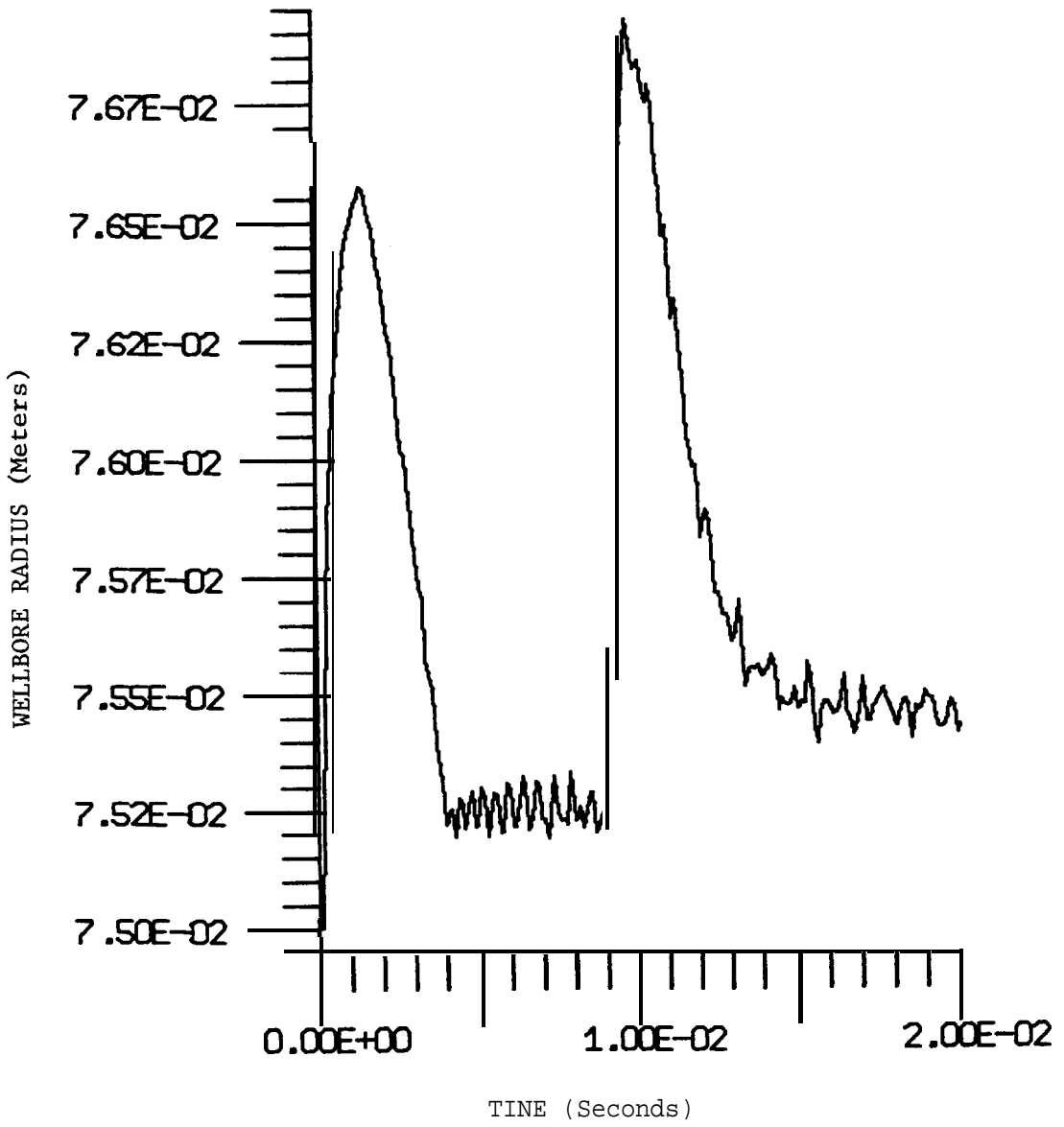


FIGURE 26. Kinefrac - Wellbore Expansion

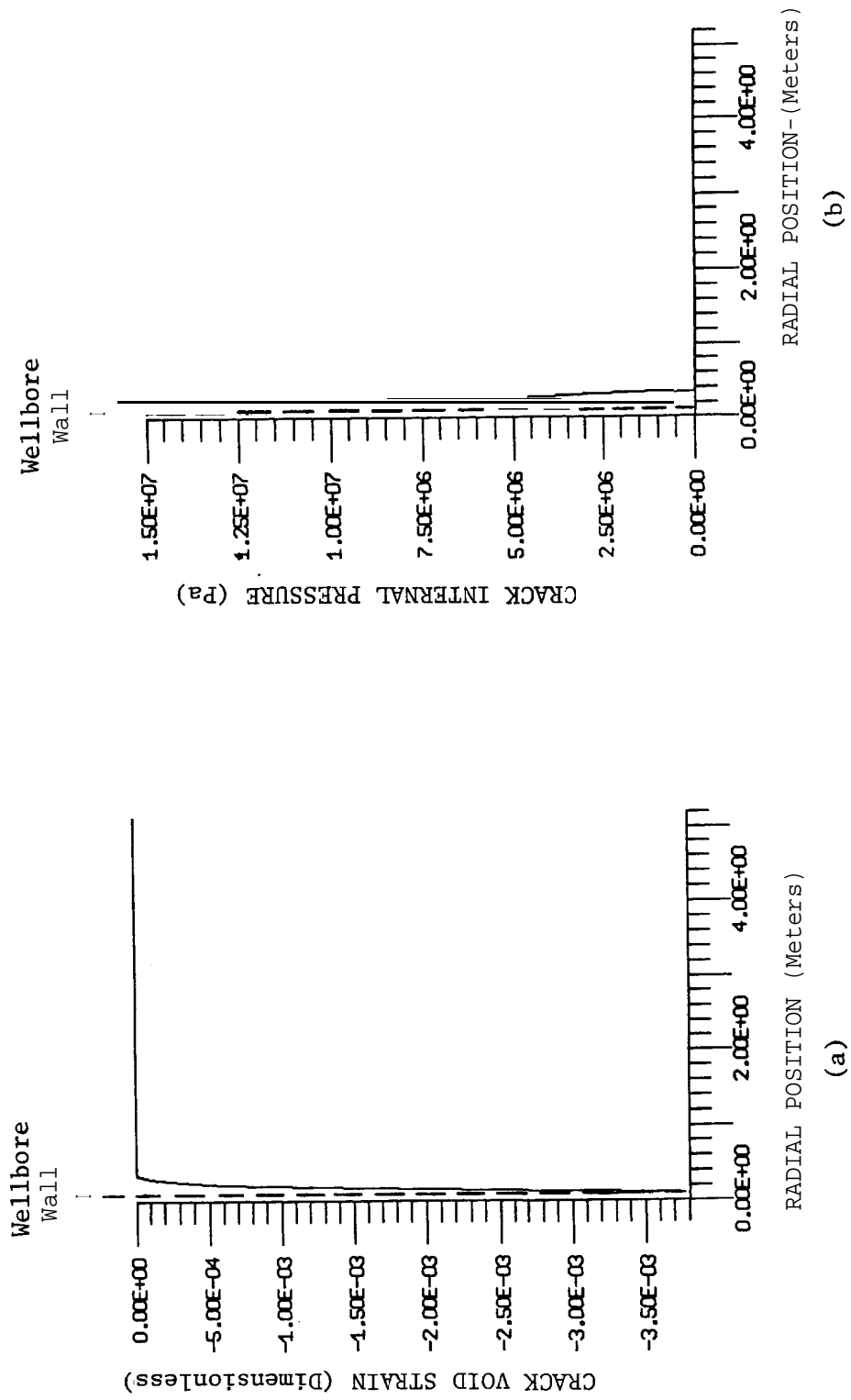
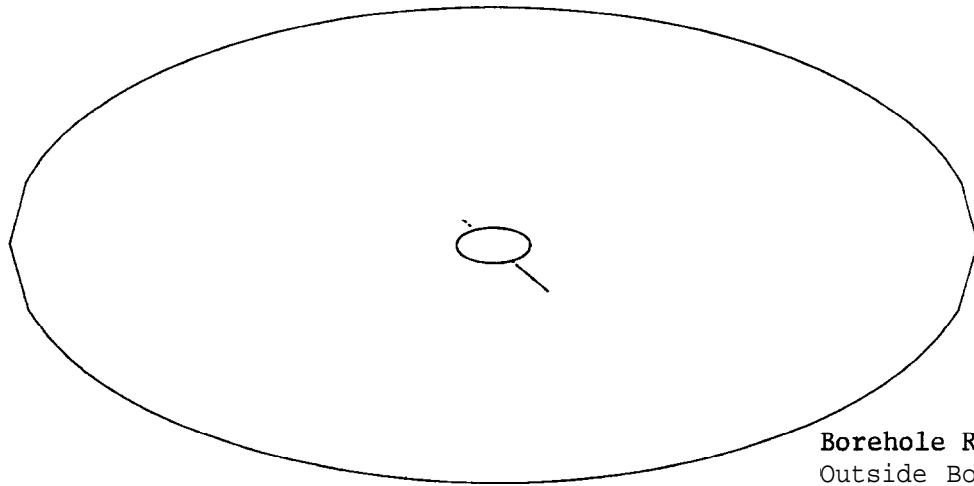
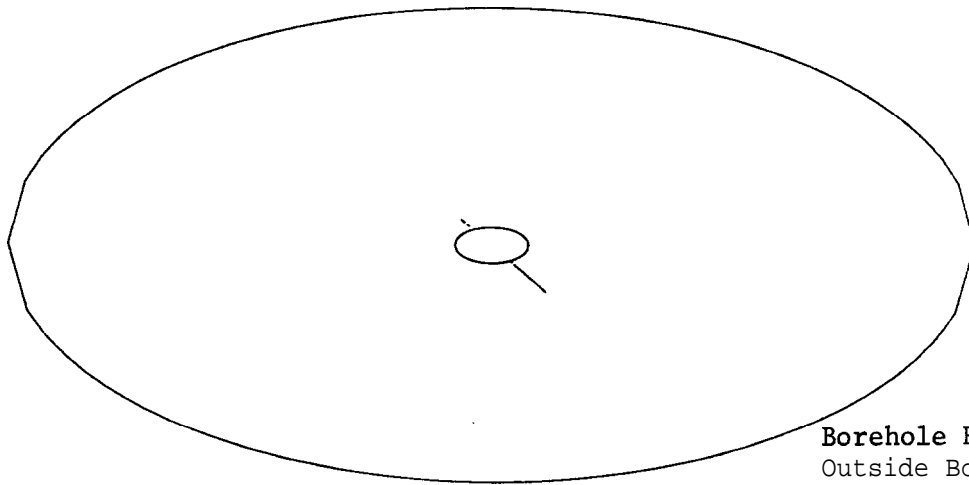


FIGURE 27. Kinefrac - Crack Void Strain Distribution and Crack Internal Pressure Profile at 16 Milliseconds



Borehole Radius = 0.1 meter
Outside Boundary = 1.0 meter

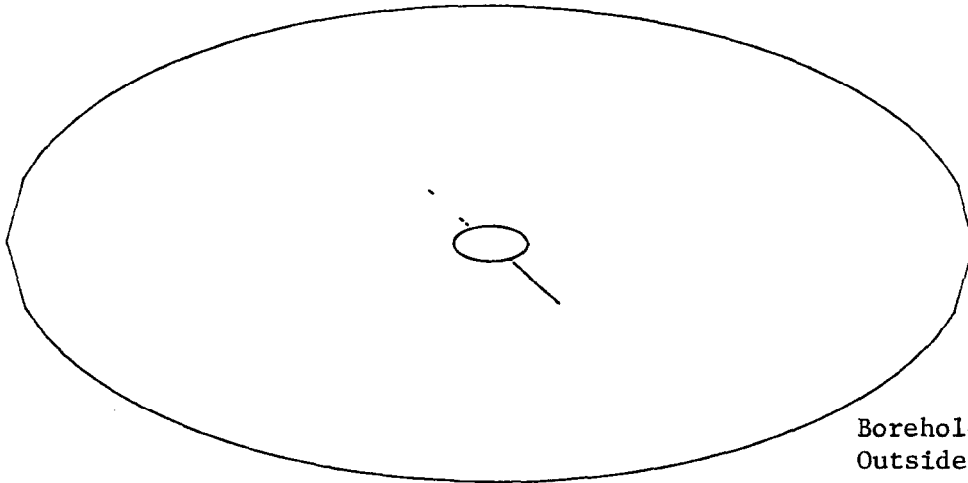
a) Radial Cracks at 3 Milliseconds



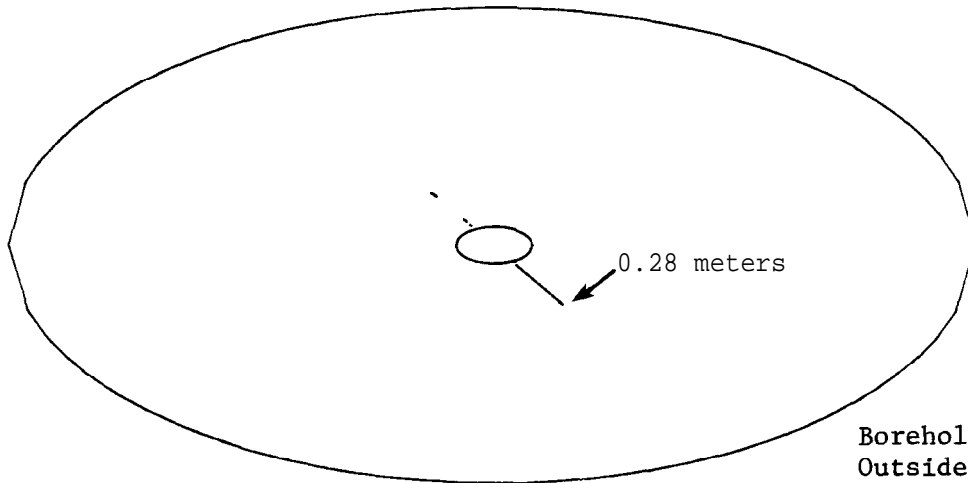
Borehole Radius = 0.1 meter
Outside Boundary = 1.0 meter

b) Radial Cracks at 5 Milliseconds

FIGURE 28. Kinefrac - CAVS Fracture Plot at 3 and 5 Milliseconds



a) Radial Cracks at 10 Milliseconds



b) Radial Cracks at 16 Milliseconds

(no additional computed cracking after 16 milliseconds)

FIGURE 29. Kinefrac - CAVS Fracture Plot at 10 and 16 Milliseconds

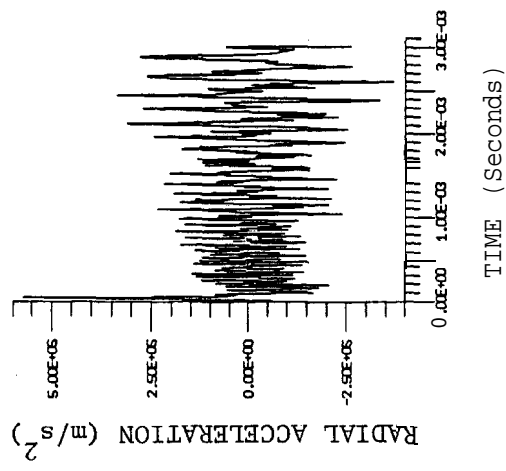
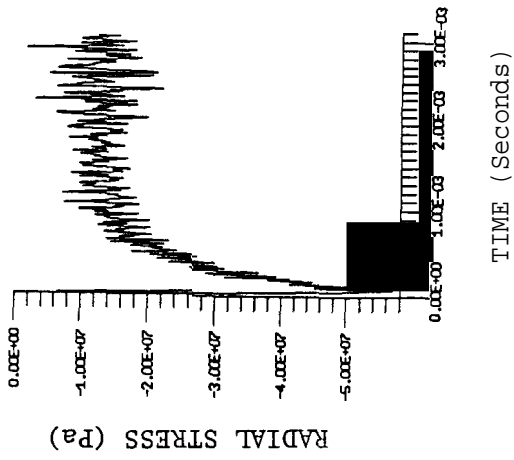
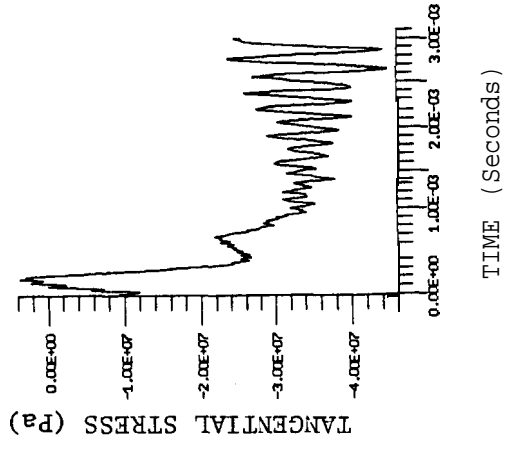


FIGURE 30. Dynafrac - Radial Acceleration, Radial Stress and Tangential Stress at Wellbore Wall

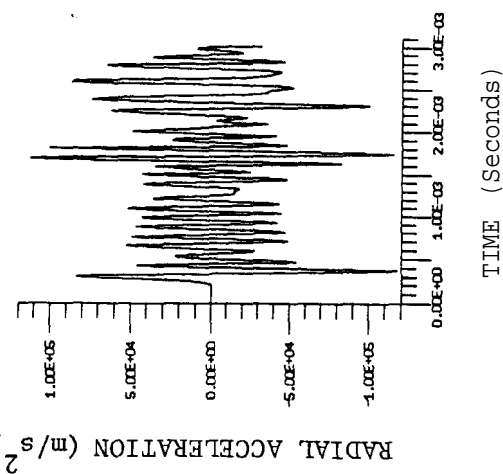
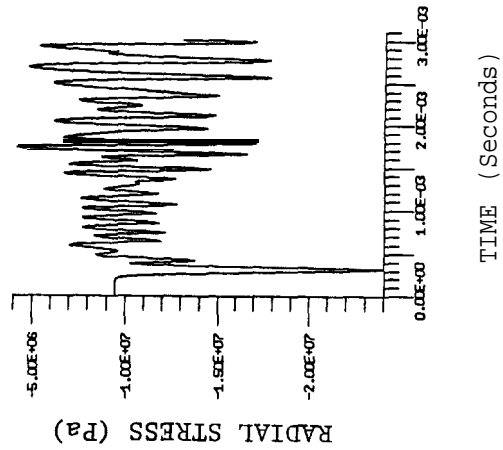
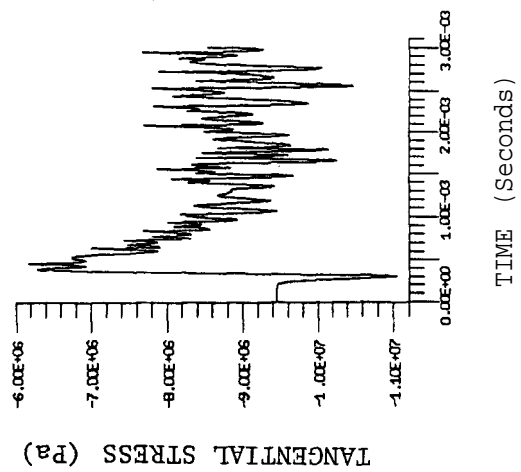


FIGURE 31. Dynafrac - Radial Acceleration, Radial Stress and Tangential Stress at Approximately 1.5 Feet from Wellbore Center

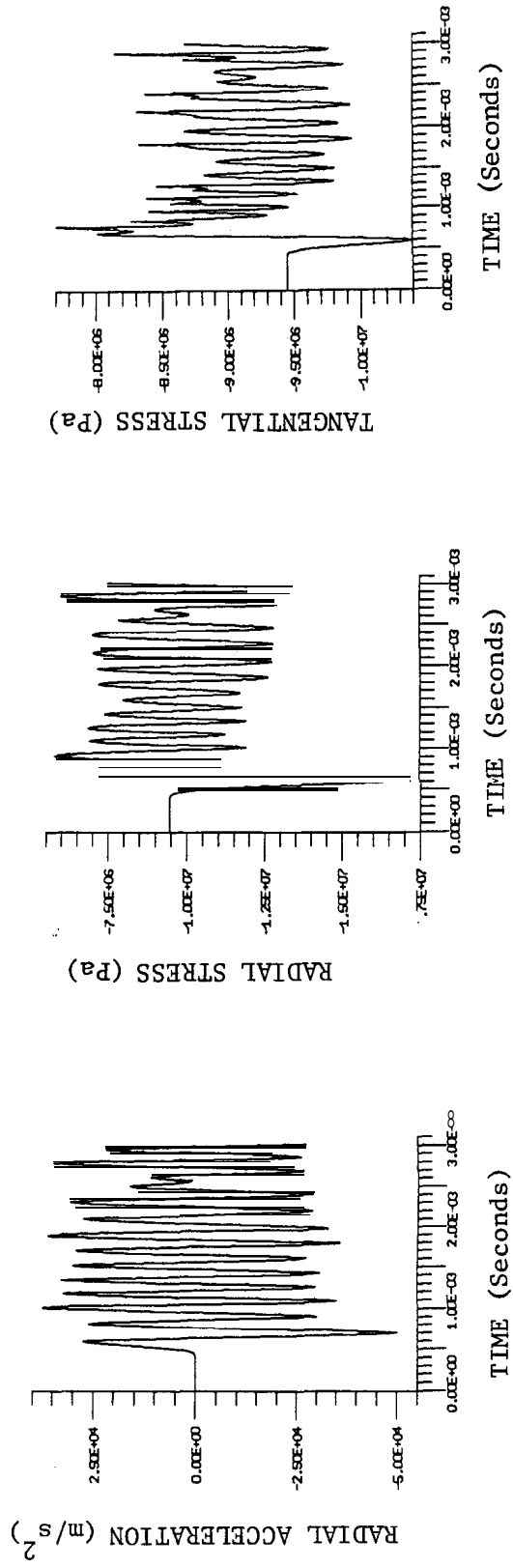


FIGURE 32. Dynafrac - Radial Acceleration, Radial Stress and Tangential Stress at Approximately 3.0 Feet from Wellbore Center

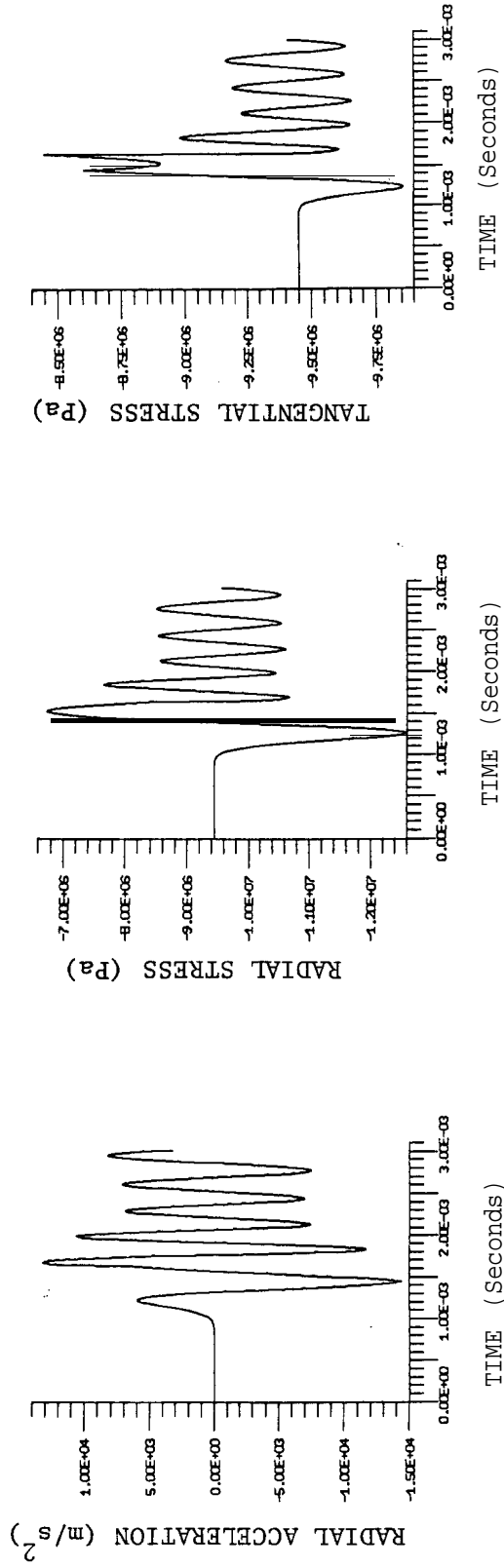


FIGURE 33. Dynafrac - Radial Acceleration, Radial Stress and Tangential Stress at Approximately 6.0 Feet from Wellbore Center

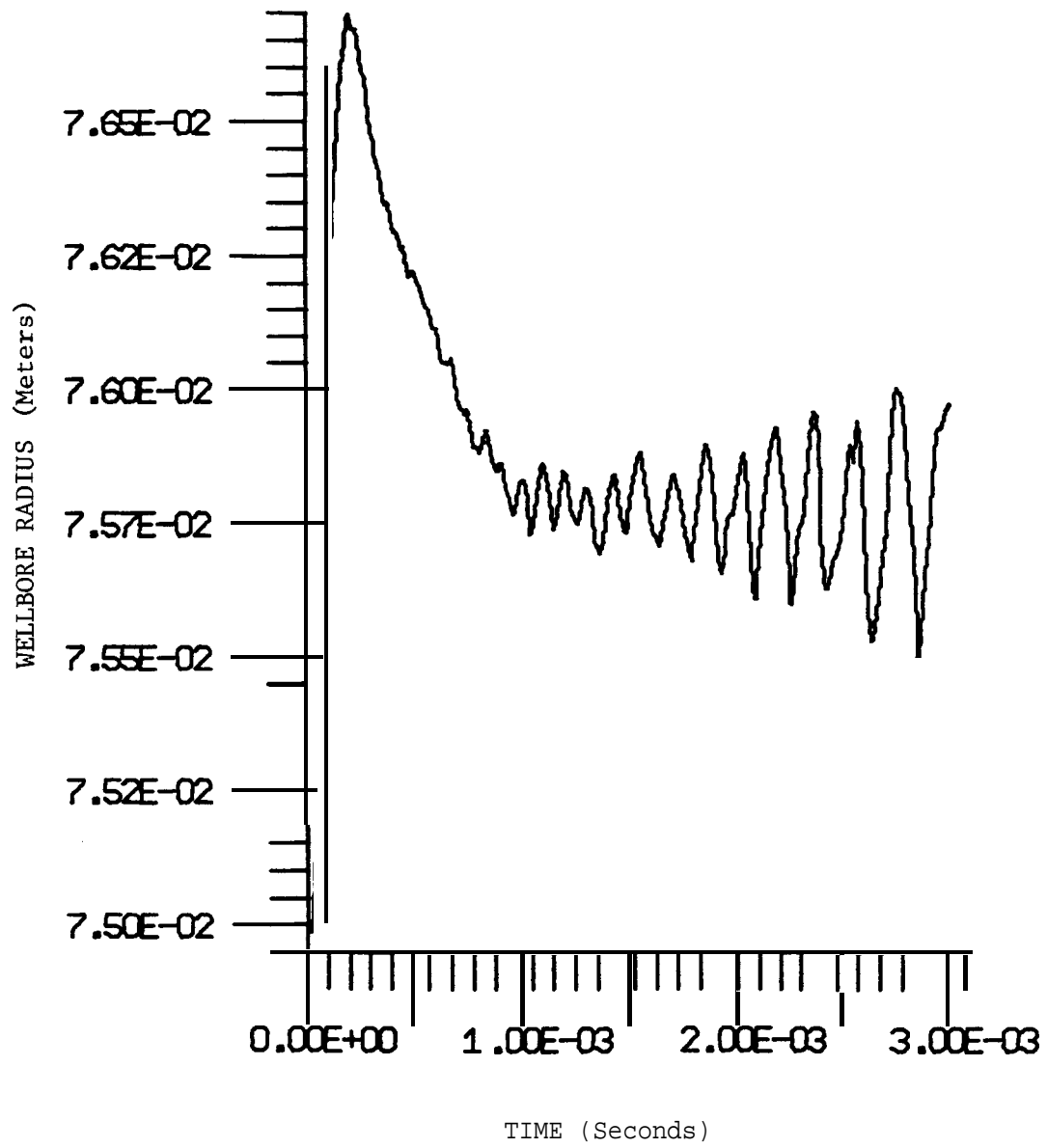


FIGURE 34. Dynafrac - Well Expansion

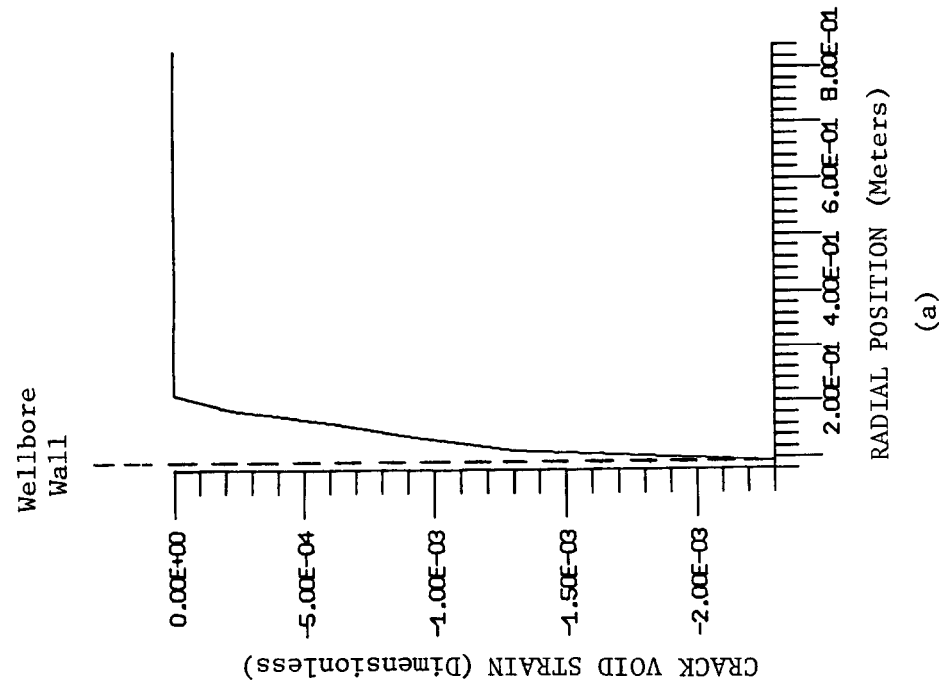
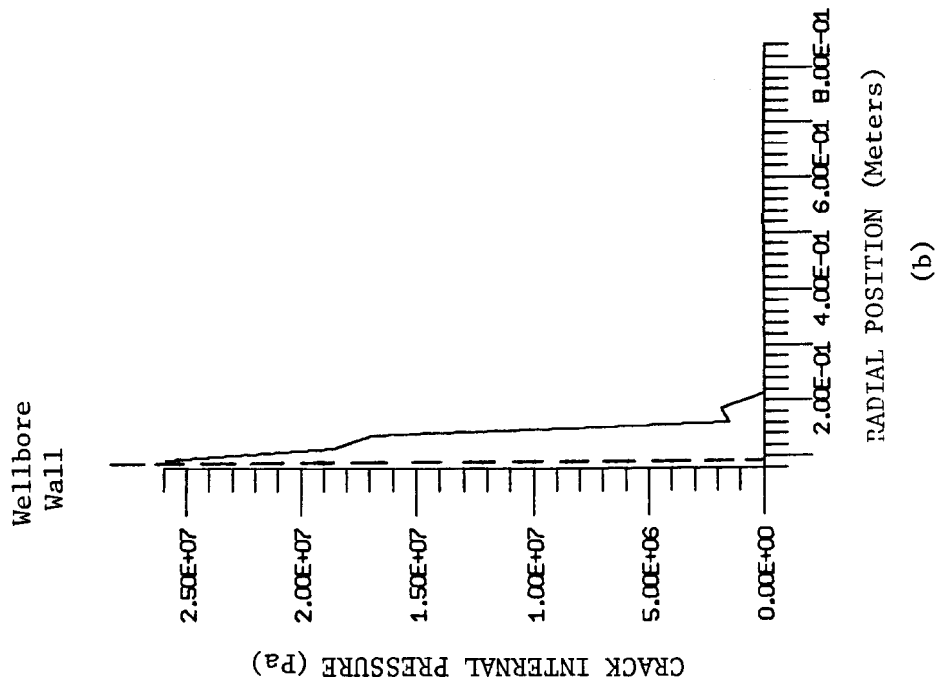


FIGURE 35. Dynafrac - Crack Void Strain Distribution and Crack Internal Pressure Profile at 0.25 Milliseconds

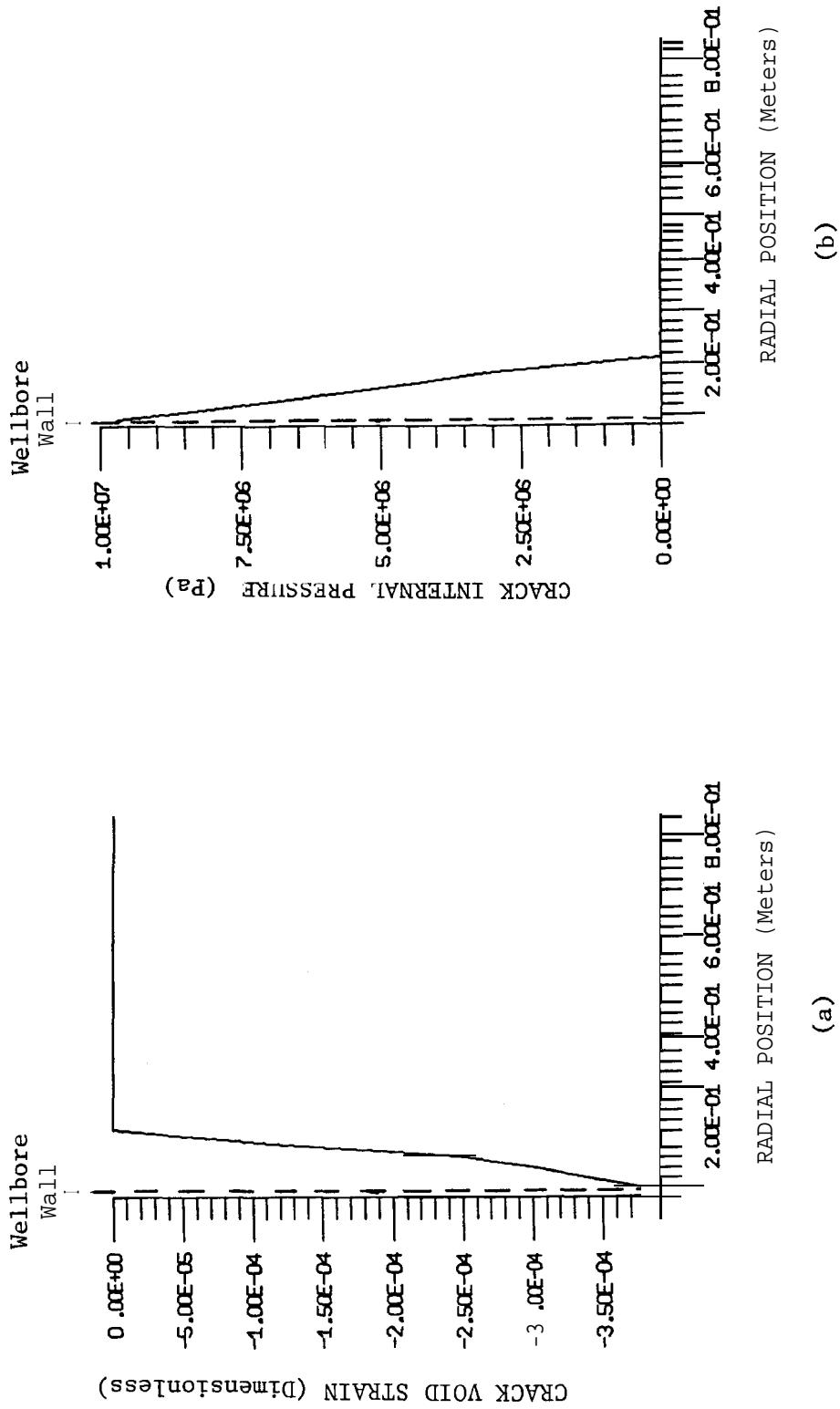
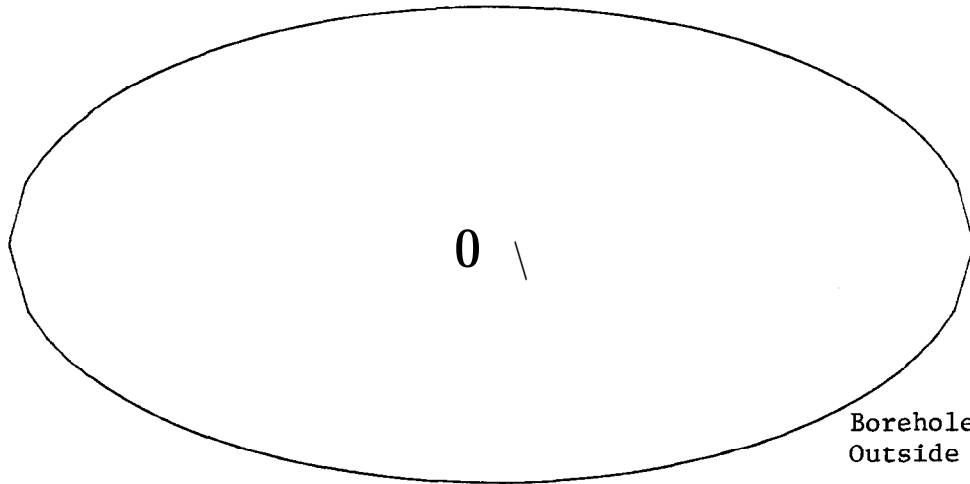
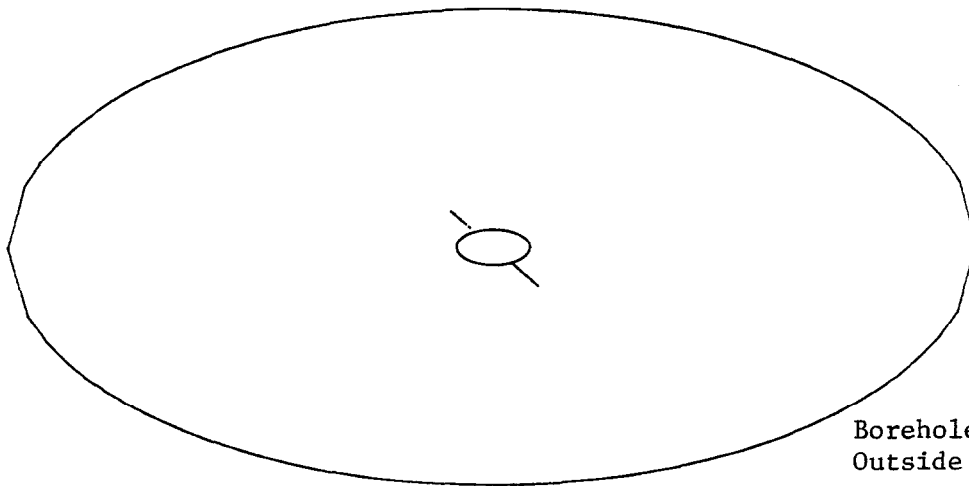


FIGURE 36. Dynafrac - Crack Void Strain Distribution and Crack Internal Pressure Profile at 2.0 Milliseconds



a) Radial Cracks at 0.25 Milliseconds



b) Radial Cracks at 2.0 Milliseconds

(no additional **computed cracking** after 2.0 milliseconds)

FIGURE 37. Dynafrac - CAVS Fracture Plot at 0.25 and 2.0 Milliseconds